

# Propagation of Slepyan's crack in a non-uniform elastic lattice

M.J. Nieves<sup>†</sup>, A.B. Movchan\*, I.S. Jones<sup>†</sup> and G.S. Mishuris<sup>‡</sup>

## Abstract

We model and derive the solution for the problem of a Mode I semi-infinite crack propagating in a discrete triangular lattice with bonds having a contrast in stiffness in the principal lattice directions. The corresponding Green's kernel is found and from this wave dispersion dependencies are obtained in explicit form. An equation of the Wiener-Hopf type is also derived and solved along the crack face, in order to compute the stress intensity factor for the semi-infinite crack. The crack stability is analysed via the evaluation of the energy release rate for different contrasts in stiffness of the bonds.

**Keywords:** inhomogeneous lattice, semi-infinite crack, Wiener-Hopf technique, energy release rate ratio, stress intensity factor.

## 1 Introduction

Models for cracks propagating in lattices have been extensively studied in [Slepyan (2002)]. As noted in [Marder and Gross (1995)], discrete models enable one to answer fundamental questions about the influence of the micro-structure on the crack motion.

It is possible to consider types of non-uniformity within a lattice, which can bring new effects in the wave dispersion and filtering properties of the structure. These non-uniformities may be caused, for example, by thermal pre-stress of a constrained lattice whose ligaments have different coefficients of thermal expansion. Linearisation near the pre-stressed state may lead to a model of a lattice with contrasting stiffnesses of bonds. Such an elastic lattice, containing a moving crack, is analysed in the present paper.

Problems involving inhomogeneous lattices containing semi-infinite cracks have been recently analysed. Examples include those containing particles of contrasting mass [Mishuris, et al. (2007)], and the dynamic extraction of a chain within the lattice [Mishuris, et al. (2008)].

The propagation of the crack may be caused by feeding waves, generated by some remote source, which lead to the breaking of subsequent bonds within the lattice. Feeding waves bring energy to the crack-front bonds which cause their disintegration one by one and this produces dissipative waves which carry energy away from the front. This process has been investigated in [Slepyan (2001a)], where Mode III crack propagation within a square-cell lattice is considered, under the assumption of uniform straight line crack growth, and steady state solutions have been obtained. The lattice is assumed to have bonds of identical stiffness which connect particles having a common mass.

The analysis of Mode I and II crack propagation in a uniform discrete triangular lattice was studied in [Slepyan (2001b)]. Compared to the case of the square-cell lattice, the equations of motion relate components of the vector field of displacements. It has been shown that both the solution to this problem and the explicit form of wave dispersion relations can be obtained.

From these lattice models, it is possible to determine the regions of crack speeds for which we have steady state crack motion, and the stability of these states can also be determined by computing the energy release rate for the crack. This has been examined in [Fineburg and Marder (1999)], [Marder and Gross (1995)] and [Marder and Liu (1993)]. Another application for a lattice problem is found in [Slepyan et al. (2010)]. Here, the model describing a structured interface along a crack with a harmonic feeding wave localised at the faces, was used to predict the position of the crack front. Numerical simulations were presented in [Mishuris, et al. (2009a), Slepyan et al. (2010)] showing that, for a given range of frequencies of the feeding wave, it was possible to have

\*Department of Mathematical Sciences, University of Liverpool, Liverpool L69 3BX, U.K.

<sup>†</sup>School of Engineering, John Moores University, James Parsons Building, Byrom Street, Liverpool L3 3AF, U.K.

<sup>‡</sup>Institute of Mathematics and Physics, Aberystwyth University, Aberystwyth, SY23 3BZ.

Corresponding author: M.J. Nieves, Email: M.J.Nieves@ljam.ac.uk, Tel: +44 151 231 2253

uniform crack growth or, in the non-linear regime of non-steady propagation, to identify an average crack speed, which is consistent with the prediction of the linear model linked to the crack propagating steadily.

The method of solution of these problems involves formulating the discrete lattice problem in terms of the Fourier transforms of functions describing the displacements [Mishuris, et al. (2009b)]. A Wiener-Hopf functional equation is then derived along the crack faces and factorised to obtain the solution. The kernel in the Wiener-Hopf equation has the interpretation of the Fourier transform of the derivatives of Green's kernel. Similar features also appear in continuum models of cracks which are solved using singular integral equation techniques. [add reference]

In this article, using the method in [Slepyan (2001b)], our main goal is to solve the problem for a discrete triangular lattice, which is constrained at infinity, containing a semi-infinite crack with additional inhomogeneities being brought by the inclined bonds having a contrast in stiffness to the horizontal bonds (see Figure 1). This contrast in stiffness may arise as an effect of thermal pre-stress, for instance, heating a lattice with bonds that have different coefficients of thermal expansion in the principal directions. The problem for a crack in the uniform triangular lattice has been studied in [Slepyan (2002), Chapter 12].

The plan of the paper is as follows. section 2 includes the description of the problem for a two dimensional lattice with a semi-infinite crack, containing particles of common mass with bonds having contrasting stiffnesses in the principal directions. In section 3, we rewrite the problem for the lattice using the continuous Fourier transform in the crack line direction, and these equations are solved for the displacements of a particle inside the lattice. A Wiener-Hopf equation for particles along the line of the crack is then written in section 4 and the representation of the kernel function of this equation is derived. An analysis of the dispersion relations obtained from the roots and poles of the kernel function is carried out in section 5. In section 6, we solve the Wiener-Hopf equation of section 4. In section 7, we evaluate the energy release rate for the crack propagating through the inhomogeneous lattice and investigate its sensitivity to the crack speed and to the stiffness contrast. We compute the stress intensity factor for the semi-infinite crack propagating through the inhomogeneous lattice and show its behaviour, for different stiffness contrasts, as a function of the crack speed in section 8. In section 9, we give conclusions on the results presented here.

In addition to the main text of the article, we also provide Appendices which include more details of the derivations of the results contained in main body of the article. In Appendix I, the coefficient of the leading order term of the asymptotics for the kernel function near the zero wavenumber is studied. Some comments relating to the analysis of the poles for the kernel function of the Wiener-Hopf equation are presented in the Appendix II. Properties of the kernel function which are necessary for its factorisation as a product of two functions, analytic in different halves of the complex plane, are proved in Appendix III. In Appendix IV, the derivation of the solution to the Wiener-Hopf equation is given. Finally, asymptotes in the vicinity of the zero wavenumber for the functions obtained after the factorisation of the kernel function are derived in Appendix V.

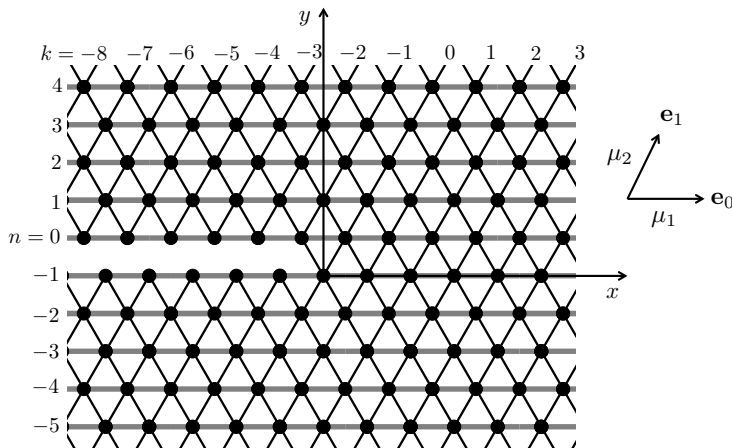


Figure 1: The inhomogeneous lattice containing a semi-infinite crack showing the lattice coordinates. The crack is located between the rows  $n = -1$  and  $n = 0$ .

## 2 Elastic lattice and the governing equations

### 2.1 The notion of Slepyan's crack

The crack in the infinite triangular lattice considered here (see Figure 1), is a semi-infinite fault which appears as the result of subsequent breakage of bonds in a straight line, and propagates with a constant speed  $V$  according to  $\eta = x - Vt$ , (e.g. between rows  $n = 0$  and  $-1$  in Figure 1). Here,  $x$  is the horizontal coordinate associated with the crack tip node, directed in the line of the propagation of the crack, and  $t$  is time. This approach to describing the crack propagation, was first used in [Slepyan (2001b)]. It allows for the reduction of the full transient problem to a simple difference problem in the vertical direction following the Fourier transform with respect to  $\eta$ , where the forces in the bonds of the lattice can be linked to the displacements and stresses through a Wiener-Hopf equation along the crack. Dispersion properties of this lattice configuration can also be obtained through the roots and poles of the kernel function involved this equation. The approach is elegant and leads to a closed form solution. One of the drawbacks is that the model does not serve the case of small crack velocities, as discussed further in the text below. However, for a finite range of values of a subsonic crack speed, one can identify a regime of steady crack propagation. In the real physical situation, crack propagation can be treated in the averaged sense, and the average crack velocity can be evaluated, as discussed in [Mishuris, et al. (2009a)].

### 2.2 Non-uniform lattice

We consider a triangular lattice containing a semi-infinite crack (see Figure 1), where horizontal bonds are assumed to have stiffness  $\mu_1$  and diagonal bonds stiffness  $\mu_2$ . In the following, the ratio of bar stiffnesses is  $\alpha = \mu_1/\mu_2$ . The length of the bonds connecting the particles is normalised to 1. All particles are assumed to have identical mass  $m$ .

To characterise the positions of masses within the lattice, it is convenient to use the basis vectors  $\mathbf{e}_0 = (1, 0)^T$  and  $\mathbf{e}_1 = (1/2, \sqrt{3}/2)^T$ . The in-plane displacement vector at the node  $\mathbf{x} = k\mathbf{e}_0 + n\mathbf{e}_1$ , where  $k, n$  are integers, is  $\mathbf{u}(t, \mathbf{x})$ . Projected displacements onto the horizontal and vertical axes, associated with the crack tip node, are denoted by  $u$  and  $v$ , respectively.

We define the constant

$$C_R = \frac{1}{2m^{1/2}} \sqrt{2\mu_1 + \mu_2 - \sqrt{3\mu_1^2 + (\mu_1 - \mu_2)^2}} \quad (2.1)$$

which will be determined, in section 5, as the Rayleigh wave speed for a wave that propagates along the crack faces aligned with the  $x$ -axis, which are traction free. The crack is assumed to propagate steadily through lattice with speed  $V \leq C_R$ , and this propagation is caused by the breaking of the bonds between rows  $n = -1$  and  $n = 0$ .

### 2.3 Normalised crack speed

Let  $V_*$  be the dimensionless crack speed defined by  $V_* = V\sqrt{m/\mu_2}$ . Since we consider sub-Rayleigh wave speed, using (2.1) we obtain

$$V_*^2 \leq g(\alpha) = \frac{C_R^2 m}{\mu_2} = \frac{2\alpha + 1 - \sqrt{3\alpha^2 + (\alpha - 1)^2}}{4}. \quad (2.2)$$

**Proposition 1** *The function  $g(\alpha)$  is increasing for  $\alpha > 0$ , with  $0 < g(\alpha) \leq 3/8$  and  $\frac{dg}{d\alpha}(\alpha) < 3/4$ .*

*Proof.* For  $g(\alpha)$ , in (2.2), we have

$$\frac{dg}{d\alpha}(\alpha) = \frac{1}{2} - \frac{4\alpha - 1}{4\sqrt{3\alpha^2 + (\alpha - 1)^2}},$$

and with  $0 < \alpha \leq 1/4$ , it is clear that  $g(\alpha)$  is an increasing function on this interval. Now, let  $\alpha > 1/4$ . Using the inequality

$$3\alpha^2 + (\alpha - 1)^2 > \frac{(4\alpha - 1)^2}{4}, \quad (2.3)$$

leads to

$$\frac{dg}{d\alpha}(\alpha) > 0, \quad \text{for } \alpha > 1/4.$$

Therefore,  $g(\alpha)$  is an increasing function for  $\alpha > 0$ , and

$$g(0) = 0, \quad \text{and} \quad g(\alpha) \leq g(\infty) = \frac{3}{8}, \quad \alpha > 0.$$

Next, owing to (2.3)

$$\frac{d^2 g}{d\alpha^2}(\alpha) = \frac{1}{4\sqrt{3\alpha^2 + (\alpha - 1)^2}} \left( \frac{(1 - 4\alpha)^2}{3\alpha^2 + (\alpha - 1)^2} - 4 \right) < 0,$$

which shows  $\frac{dg}{d\alpha}(\alpha)$  is a decreasing function, that takes its maximum as  $\alpha \rightarrow 0$ :

$$\frac{dg}{d\alpha}(0) = \frac{3}{4}.$$

□

## 2.4 Dynamic equations for the lattice above the crack

The equations of motion for a particle inside the lattice ( $n > 0$ ) are:

$$m\ddot{\mathbf{u}} = \mu_1 \mathbf{e}_0 \cdot \left\{ \mathbf{u}|_{\mathbf{x}+\mathbf{e}_0} - \mathbf{u}|_{\mathbf{x}-\mathbf{e}_0} - 2\mathbf{u}|_{\mathbf{x}} \right\} \mathbf{e}_0 + \mu_2 \sum_{j=1,2} \mathbf{v}_j \cdot \left\{ \mathbf{u}|_{\mathbf{x}+\mathbf{v}_j} + \mathbf{u}|_{\mathbf{x}-\mathbf{v}_j} - 2\mathbf{u}|_{\mathbf{x}} \right\} \mathbf{v}_j. \quad (2.4)$$

where  $\mathbf{v}_1 = \mathbf{e}_1$  and  $\mathbf{v}_2 = \mathbf{e}_1 - \mathbf{e}_0$ .

Making a change of variable to the moving coordinate system, we set  $\eta = x - Vt$ . Then (2.4) in terms of projected displacements becomes

$$\begin{aligned} & \frac{mV^2}{\mu_2} \frac{d^2 u}{d\eta^2}(\eta, n) - \frac{1}{4} [u(\eta + 1/2, n + 1) + u(\eta - 1/2, n + 1) + u(\eta + 1/2, n - 1) + u(\eta - 1/2, n - 1)] \\ & - \frac{\sqrt{3}}{4} [v(\eta + 1/2, n + 1) - v(\eta - 1/2, n + 1) + v(\eta - 1/2, n - 1) - v(\eta + 1/2, n - 1)] \\ & - \alpha [u(\eta + 1, n) + u(\eta - 1, n)] + (1 + 2\alpha)u(\eta, n) = 0, \end{aligned}$$

and

$$\begin{aligned} & \frac{mV^2}{\mu_2} \frac{d^2 v}{d\eta^2}(\eta, n) - \frac{\sqrt{3}}{4} [u(\eta + 1/2, n + 1) - u(\eta - 1/2, n + 1) - u(\eta + 1/2, n - 1) + u(\eta - 1/2, n - 1)] \\ & - \frac{3}{4} [v(\eta + 1/2, n + 1) + v(\eta - 1/2, n + 1) + v(\eta + 1/2, n - 1) + v(\eta - 1/2, n - 1)] + 3v(\eta, n) = 0, \end{aligned}$$

where  $u(\eta, n)$  and  $v(\eta, n)$  are the components of the displacement vector  $\mathbf{u}$ , along row  $n$  after the change of variable.

## 3 Solution for the lattice half-plane

Here, for the intact part of the lattice ( $n > 0$ ) we will obtain the solution to the problem of section 2.4. We follow the method discussed in [Slepyan (2001b)], which makes use of the continuous Fourier transforms  $u^F$  and  $v^F$  with respect to the moving coordinate associated with the crack.

### 3.1 The continuous Fourier transform of the system

We take the Fourier transform with respect to  $\eta$ , and obtain

$$\begin{aligned} & [u^F(\xi, n + 1) + u^F(\xi, n - 1)] \cos(\xi/2) - 2[1 + 2\alpha(1 - \cos(\xi)) + m(\varepsilon + i\xi V)^2/\mu_2] u^F(\xi, n) \\ & - i\sqrt{3} \sin(k/2) [v^F(\xi, n + 1) - v^F(\xi, n - 1)] = 0, \end{aligned} \quad (3.1)$$

$$\begin{aligned} & 3[v^F(\xi, n + 1) + v^F(\xi, n - 1)] \cos(\xi/2) - 2[3 + m(\varepsilon + i\xi V)^2/\mu_2] v^F(\xi, n) \\ & - i\sqrt{3} \sin(\xi/2) [u^F(\xi, n + 1) - u^F(\xi, n - 1)] = 0, \end{aligned} \quad (3.2)$$

where  $\varepsilon$  is the regularization parameter,  $0 < \varepsilon \ll 1$ .

### 3.2 General solution for the half-plane lattice

The functions  $u^F$  and  $v^F$  are sought in the form

$$u^F = C\Lambda^n \quad \text{and} \quad v^F = D\Lambda^n .$$

Insertion of these into (3.1) and (3.2) yield

$$C\{(\Lambda + 1/\Lambda)\cos(\xi/2) - 2[1 + 2\alpha(1 - \cos(\xi)) + m(\varepsilon + i\xi V)^2/\mu_2]\} - i\sqrt{3}\sin(\xi/2)(\Lambda - 1/\Lambda)D = 0 ,$$

$$D\{3(\Lambda + 1/\Lambda)\cos(\xi/2) - 2(3 + Y)\} - i\sqrt{3}\sin(\xi/2)(\Lambda - 1/\Lambda)C = 0 .$$

For non-trivial solutions of  $C$  and  $D$ , the biquadratic equation in terms of  $\Lambda$  must be satisfied:

$$\begin{aligned} & (\Lambda + 1/\Lambda)^2 - 2\{2 + 2\alpha(1 - \cos(\xi)) + \frac{4}{3\mu_2}m(\varepsilon + i\xi V)^2\}(\Lambda + 1/\Lambda)\cos(\xi/2) \\ & + 2\{1 + \cos(\xi) + 4\alpha(1 - \cos(\xi))\} + \frac{4}{3\mu_2}m(\varepsilon + i\xi V)^2\{4 + 2\alpha(1 - \cos(\xi)) + \frac{m}{\mu_2}(\varepsilon + i\xi V)^2\} = 0 . \end{aligned} \quad (3.3)$$

We require that  $|\Lambda| \leq 1$ , and this leads to the solutions

$$\Lambda_j = z_j \pm \sqrt{z_j^2 - 1} , \quad j = 1, 2, \quad (3.4)$$

where the sign in front of the square root in  $\Lambda_j$  has to be chosen so that the condition  $|\Lambda_j| \leq 1$ ,  $j = 1, 2$ , for  $\xi \in \mathbb{R}$  and  $V > 0$ , is satisfied. For  $j = 1, 2$

$$\begin{aligned} z_j &= \left(1 + 2\alpha\sin^2(\xi/2) + \frac{2m(\varepsilon + i\xi V)^2}{3\mu_2}\right)\cos(\xi/2) \\ &+ (-1)^j \left[ \frac{m^2(\varepsilon + i\xi V)^4}{9\mu_2^2} - 4\sin^2(\xi/2) \left( \alpha\sin^2(\xi/2) + \frac{m(\varepsilon + i\xi V)^2}{3\mu_2} \right) \right. \\ &\times \left. \left( \alpha\sin^2(\xi/2) + \frac{m(\varepsilon + i\xi V)^2}{3\mu_2} + 1 - \alpha \right) \right]^{1/2} . \end{aligned} \quad (3.5)$$

Then for  $n > 0$ , with such choices of  $\Lambda$ , the Fourier transforms of the displacements have the form

$$\begin{pmatrix} u^F(\xi, n) \\ v^F(\xi, n) \end{pmatrix} = \frac{1}{f_v(\Lambda_1)f_v(\Lambda_2)} \begin{pmatrix} f_v(\Lambda_1)f_v(\Lambda_2) & f_v(\Lambda_1)f_v(\Lambda_2) \\ -if_u(\Lambda_1)f_v(\Lambda_2) & -if_u(\Lambda_2)f_v(\Lambda_1) \end{pmatrix} \begin{pmatrix} C_1\Lambda_1^n \\ C_2\Lambda_2^n \end{pmatrix} \quad (3.6)$$

where

$$f_u(\Lambda) = -\sqrt{3}\sin(\xi/2)(\Lambda^2 - 1) \quad \text{and} \quad f_v(\Lambda) = 3(\Lambda^2 + 1)\cos(\xi/2) - 2\Lambda(3 + m(\varepsilon + i\xi V)^2/\mu_2) .$$

### 3.3 Mode I Symmetry conditions

For Mode I, using the symmetry relations

$$u(\eta, -n - 1) = u(\eta, n) , \quad v(\eta, -n - 1) = -v(\eta, n) , \quad (3.7)$$

we can extend the solution in the upper half-plane (3.6) to the lower half-plane. Then, for  $n \leq -1$ , the Fourier transforms of the horizontal and vertical displacements are

$$\begin{pmatrix} u^F(\xi, n) \\ v^F(\xi, n) \end{pmatrix} = \frac{1}{f_v(\Lambda_1)f_v(\Lambda_2)} \begin{pmatrix} f_v(\Lambda_1)f_v(\Lambda_2) & f_v(\Lambda_1)f_v(\Lambda_2) \\ if_u(\Lambda_1)f_v(\Lambda_2) & if_u(\Lambda_2)f_v(\Lambda_1) \end{pmatrix} \begin{pmatrix} C_1\Lambda_1^{-n-1} \\ C_2\Lambda_2^{-n-1} \end{pmatrix} .$$

The forces in the bonds directed along  $-\mathbf{e}_1$  and  $\mathbf{e}_0 - \mathbf{e}_1$ , respectively, for a node in the upper half-plane of the lattice, have the form

$$\mathcal{S}(\eta, n) = \frac{1}{2}[u(\eta, n) - u(\eta - 1/2, n - 1)] + \frac{\sqrt{3}}{2}[v(\eta, n) - v(\eta - 1/2, n - 1)] , \quad (3.8)$$

$$\mathcal{T}(\eta, n) = \frac{1}{2}[u(\eta + 1/2, n - 1) - u(\eta, n)] + \frac{\sqrt{3}}{2}[v(\eta, n) - v(\eta + 1/2, n - 1)] . \quad (3.9)$$

The conditions (3.7) also give

$$\mathcal{S}(\eta, 0) = \frac{1}{2}[u(\eta, 0) - u(\eta - 1/2, 0)] + \frac{\sqrt{3}}{2}[v(\eta, 0) + v(\eta - 1/2, 0)] , \quad \mathcal{T}(\eta, 0) = \mathcal{S}(\eta + 1/2, 0)$$

or

$$\mathcal{S}^F(\xi, 0) = \frac{1}{2}(1 - e^{i\xi/2})u^F(\xi, 0) + \frac{\sqrt{3}}{2}(1 + e^{i\xi/2})v^F(\xi, 0) , \quad \mathcal{T}^F(\xi, 0) = \mathcal{S}^F(\xi, 0)e^{-i\xi/2} . \quad (3.10)$$

The representation (3.6), then allows  $\mathcal{S}^F$  in (3.10) to be rewritten as

$$\mathcal{S}^F(\xi, 0) = \frac{1}{2f_v(\Lambda_1)f_v(\Lambda_2)}\mathbf{R}^T\mathbf{T}\mathbf{B}(\Lambda_1, \Lambda_2)\mathbf{C} , \quad (3.11)$$

with

$$\mathbf{C} = \begin{pmatrix} C_1 \\ C_2 \end{pmatrix} , \quad \mathbf{R} = \begin{pmatrix} 1 - e^{i\xi/2} \\ i(1 + e^{i\xi/2}) \end{pmatrix} ,$$

and

$$\mathbf{T} = \begin{pmatrix} 1 & 0 \\ 0 & \sqrt{3} \end{pmatrix} , \quad \mathbf{B}(\Lambda_1, \Lambda_2) = \begin{pmatrix} f_v(\Lambda_1)f_v(\Lambda_2) & f_v(\Lambda_1)f_v(\Lambda_2) \\ -f_u(\Lambda_1)f_v(\Lambda_2) & -f_u(\Lambda_2)f_v(\Lambda_1) \end{pmatrix} .$$

## 4 The Wiener-Hopf equation along the crack

In this section, we will use the equations of motion for a particle on the upper crack face ( $n = 0$ ), to derive a Wiener-Hopf equation. The kernel function of this equation is also obtained and its properties are investigated. This function is used in (a) section 5 for analysing the dispersion properties of the lattice and (b) for computing the energy release rate of the propagating crack in section 7.

### 4.1 Dynamic equations along the crack face ( $n = 0$ )

Now we consider the equations of motion for particles along  $n = 0$ . The equations are similar to those presented in section 2.4. However, since particles along the crack face have no bonds corresponding to the vectors  $-\mathbf{e}_1$  and  $\mathbf{e}_0 - \mathbf{e}_1$ , and are acted on by an external force  $\phi$  (see Figure 2), this should be taken into account.

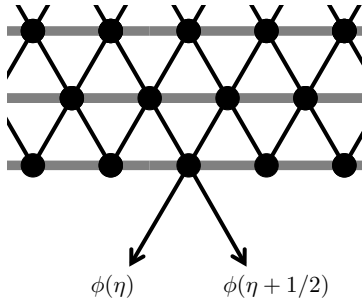


Figure 2: The particles along the crack face at  $n = 0$ , acted on by external forces  $\phi(\eta)$  and  $\phi(\eta + 1/2)$ .

Ahead of the crack, for particles along  $n = 0$ , the elongation of the bonds corresponding to  $\mathbf{e}_0$ ,  $\mathbf{e}_1$ ,  $\mathbf{e}_1 - \mathbf{e}_0$  and  $-\mathbf{e}_0$  are the same as those for a particle in the intact upper lattice half plane. Also the internal force of the bond in the direction of  $-\mathbf{e}_1$ , can be written as

$$\mathcal{M}(\eta, 0) = \mathcal{S}(\eta)H(\eta), \quad \mathcal{M}^F = \mathcal{S}_+, \quad (4.1)$$

where  $H$  is the Heaviside function. Using (3.10) and  $\mathcal{M}^F$ , a similar expression for the internal force in the bond directed along  $\mathbf{e}_0 - \mathbf{e}_1$  is obtained,  $\mathcal{N}^F = \mathcal{S}_+ e^{-ik/2}$ . The external forces acting on the particles on the line  $n = 0$ , from (3.10), have the form  $\phi(\eta)$  and  $\phi(\eta + 1/2)$ , which are directed along  $-\mathbf{e}_1$  and  $\mathbf{e}_0 - \mathbf{e}_1$ , respectively.

Then, the Fourier transform of the equations of motion for the particles along the line  $n = 0$  are

$$\begin{aligned} \frac{m}{\mu_2}(\varepsilon + i\xi V)^2 u^F(\xi, 0) &= \frac{1}{2} \cos(\xi/2) u^F(\xi, 1) - \{2\alpha(1 - \cos(\xi/2)) + 1/2\} u^F(\xi, 0) \\ &\quad - \frac{i\sqrt{3}}{2} \sin(\xi/2) v^F(\xi, 1) - \frac{1}{2}(1 - e^{-ik/2})(\mathcal{S}_+ + \phi^F), \end{aligned}$$

$$\frac{m}{\mu_2}(\varepsilon + i\xi V)^2 v^F(k, 0) = -\frac{i\sqrt{3}}{4} \sin(\xi/2) u^F(\xi, 1) + \frac{3}{4} \cos(\xi/2) v^F(\xi, 1) - \frac{3}{2} v^F(\xi, 0) - \frac{\sqrt{3}}{2}(1 + e^{-ik/2})(\mathcal{S}_+ + \phi^F).$$

In order that the expressions (3.6) fulfill these equations, the system

$$\mathcal{T}^F(\xi, 0) - \mathcal{S}^F(\xi, 0) = -(1 - e^{-i\xi/2})(\mathcal{S}_+ + \phi^F), \quad \mathcal{T}^F(\xi, 0) + \mathcal{S}^F(\xi, 0) = (1 + e^{-i\xi/2})(\mathcal{S}_+ + \phi^F),$$

should be satisfied (see (3.1), (3.2) and (3.10)). Using the representation (3.6) for the displacements when  $n \geq 0$ , in the above, leads to

$$\Xi(\Lambda_1, \Lambda_2) \mathbf{C} = -\Lambda_1 \Lambda_2 f_v(\Lambda_1) f_v(\Lambda_2) \bar{\mathbf{R}}(\mathcal{S}_+ + \phi^F).$$

where the matrix  $\Xi(\Lambda_1, \Lambda_2) = [\Xi_{ij}(\Lambda_1, \Lambda_2)]_{i,j=1}^2$  has the entries

$$\begin{aligned} \Xi_{11}(\Lambda_1, \Lambda_2) &= \Lambda_1 f_v(\Lambda_2) (f_v(\Lambda_1) (\cos(\xi/2) - \Lambda_1) + \sqrt{3} \sin(\xi/2) f_v(\Lambda_1)), \\ \Xi_{21}(\Lambda_1, \Lambda_2) &= \Lambda_2 f_v(\Lambda_1) (-\sqrt{3} f_u(\Lambda_1) (\cos(\xi/2) - \Lambda_1) + f_v(\Lambda_1) \sin(\xi/2)), \\ \Xi_{12}(\Lambda_1, \Lambda_2) &= \Xi_{11}(\Lambda_2, \Lambda_1) \quad \text{and} \quad \Xi_{22}(\Lambda_1, \Lambda_2) = \Xi_{21}(\Lambda_2, \Lambda_1). \end{aligned}$$

Therefore

$$\mathbf{C} = -\Lambda_1 \Lambda_2 f_v(\Lambda_1) f_v(\Lambda_2) [\Xi(\Lambda_1, \Lambda_2)]^{-1} \bar{\mathbf{R}}(\mathcal{S}_+ + \phi^F).$$

Combining this with (3.11) yields

$$\mathcal{S}^F(\xi, 0) = -\frac{\Lambda_1 \Lambda_2}{2 \det(\Xi(\Lambda_1, \Lambda_2))} \mathbf{R}^T \boldsymbol{\Omega}(\Lambda_1, \Lambda_2) \bar{\mathbf{R}}(\mathcal{S}_+ + \phi^F). \quad (4.2)$$

with

$$\boldsymbol{\Omega}(\Lambda_1, \Lambda_2) = \mathbf{T} \mathbf{B}(\Lambda_1, \Lambda_2) \text{adj}(\Xi(\Lambda_1, \Lambda_2)),$$

and

$$\text{adj}(\Xi(\Lambda_1, \Lambda_2)) = \begin{pmatrix} \Xi_{21}(\Lambda_2, \Lambda_1) & -\Xi_{11}(\Lambda_2, \Lambda_1) \\ -\Xi_{21}(\Lambda_1, \Lambda_2) & \Xi_{11}(\Lambda_1, \Lambda_2) \end{pmatrix}, \quad (4.3)$$

$$\det(\Xi(\Lambda_1, \Lambda_2)) = \Xi_{11}(\Lambda_1, \Lambda_2) \Xi_{21}(\Lambda_2, \Lambda_1) - \Xi_{11}(\Lambda_2, \Lambda_1) \Xi_{21}(\Lambda_1, \Lambda_2).$$

Since

$$\text{adj}(\Xi(\Lambda_2, \Lambda_1)) = - \begin{pmatrix} 0 & 1 \\ 1 & 0 \end{pmatrix} \text{adj}(\Xi(\Lambda_1, \Lambda_2)), \quad \mathbf{B}(\Lambda_2, \Lambda_1) = \mathbf{B}(\Lambda_1, \Lambda_2) \begin{pmatrix} 0 & 1 \\ 1 & 0 \end{pmatrix},$$

the matrix  $\boldsymbol{\Omega}$  matrix satisfies the relation

$$\boldsymbol{\Omega}(\Lambda_1, \Lambda_2) = -\boldsymbol{\Omega}(\Lambda_2, \Lambda_1). \quad (4.4)$$

## 4.2 The Wiener-Hopf equation

Next we set

$$\mathcal{S}^F(\xi, 0) = \mathcal{S}_+ + \mathcal{S}_- ,$$

where  $\mathcal{S}_+$ ,  $\mathcal{S}_-$  are functions analytic in the upper and lower half-planes of the complex plane  $\xi$ , and as in (4.1),  $\mathcal{M}^F(\xi, 0) = \mathcal{S}_+$ , whereas the quantity  $\mathcal{S}^F$  satisfies (3.11). After inserting this into (4.2), we obtain an equation of the form

$$L(\xi)\mathcal{S}_+ + \mathcal{S}_- = (1 - L(\xi))\phi^F . \quad (4.5)$$

Here,

$$L(\xi) = 1 + \frac{\Lambda_1 \Lambda_2}{2 \det(\Xi(\Lambda_1, \Lambda_2))} \mathbf{R}^T \mathbf{\Omega}(\Lambda_1, \Lambda_2) \overline{\mathbf{R}} ,$$

where  $\Lambda_j$ ,  $j = 1, 2$ , are given in (3.4).

We note that due to (4.4) and the antisymmetry of  $\det(\Xi(\Lambda_1, \Lambda_2))$  in (4.3) with respect to  $\Lambda_1$  and  $\Lambda_2$ , that  $L(\xi)$  is symmetric with respect to  $\Lambda_1$  and  $\Lambda_2$ . We put

$$\Lambda_j^* = z_j - \sqrt{z_j^2 - 1} , j = 1, 2 ,$$

and then an equivalent representation for  $L(\xi)$  in terms of  $z_1$  and  $z_2$  (see (3.4) and (3.5)) is given by

$$L(\xi) = \frac{3r(\Lambda_1^*)r(\Lambda_2^*)(z_2 - z_1)\sqrt{z_1^2 - 1}\sqrt{z_2^2 - 1}}{r(\Lambda_1^*)F(z_2)\sqrt{z_1^2 - 1} - r(\Lambda_2^*)F(z_1)\sqrt{z_2^2 - 1}} , \quad (4.6)$$

where

$$r(\Lambda) = \begin{cases} 1, & |\Lambda| \leq 1 , \\ -1, & \text{otherwise,} \end{cases}$$

$$F(z) = 3(\cos(\xi/2) - z)^2 + 6\alpha \sin^2(\xi/2)(1 + \cos(\xi/2))(1 - z) \\ + \frac{m}{\mu_2}(\varepsilon + i\xi V)^2[1 - z \cos(\xi/2) + (1 + \cos(\xi/2))(1 - z)] .$$

The representation for  $L(\xi)$  in (4.6), contains the stiffness contrast parameter  $\alpha$  which is found in the function  $F$ . For the case  $\alpha = 1$ , (4.6) is similar to (12.47) of [Slepyan (2002), Section 12.3.5], with the only difference here being that the functions  $r(\Lambda_1^*)$ ,  $r(\Lambda_2^*)$  have been included to indicate the change of the branch cuts of the square roots whenever  $|\Lambda_{1,2}| > 1$ .

In the derivation of (4.6), from (3.4) we used

$$\Lambda_j = z_j - r(\Lambda_j^*)\sqrt{z_j^2 - 1} ,$$

together with fact

$$\frac{1}{\Lambda_j} = z_j + r(\Lambda_j^*)\sqrt{z_j^2 - 1} , \quad \text{for } j = 1, 2 .$$

## 4.3 Asymptotics of $\Lambda_{1,2}$

Here, we obtain estimates for the behaviour of the roots of (3.3), in the neighbourhood of zero and infinity, and discuss their properties.

For the auxiliary functions  $z_j$ ,  $j = 1, 2$  we have

$$z_j = \frac{m(\varepsilon + i\xi V)^2}{3\mu_2} \left[ 2 \cos(\xi/2) + (-1)^j \sqrt{1 - 4 \sin^2(\xi/2)} \right] + O(Y_q^{1/2}), \quad j = 1, 2 , \quad \xi \rightarrow \pm\infty , \quad (4.7)$$

where the term in the parenthesis is non-zero for all  $\xi$ . Here,  $Y_q = O((\varepsilon + i\xi V)^2)$  for most values of  $\xi$ , however for a periodic sequence of  $\xi = \xi_m$  we have this is  $Y_q = O(1)$ .



In the other limit,  $\xi \rightarrow 0$ , we obtain

$$z_j = 1 + \frac{1}{24}d_j\xi^2 + O(\xi^4), \quad \xi \rightarrow 0,$$

$$\sqrt{z_j^2 - 1} = \frac{\sqrt{3}\xi}{6}\sqrt{d_j} + O(|\xi|^3), \quad j = 1, 2, \quad (4.8)$$

where

$$d_j = 3(4\alpha - 1) - 16V_*^2 + (-1)^j 4M_0, \quad j = 1, 2, \quad (4.9)$$

$$M_0 = \sqrt{4V_*^4 + 3(\alpha - 1)(3\alpha - 4V_*^2)}, \quad (4.10)$$

and  $V_* = V\sqrt{m/\mu_2}$ , as above.

Now we consider the behaviour of  $\Lambda_{1,2}$  at infinity, we have

$$\Lambda_j = \frac{1}{2z_j} + O(|z_j|^{-3}), \quad |\xi| \rightarrow \infty, \quad (4.11)$$

that is,  $\Lambda_j = O(\xi^{-2})$  as  $|\xi| \rightarrow \infty$  and here the sign in front of the square root in (3.4) is chosen to maintain the condition  $|\Lambda_j| \leq 1$ ,  $j = 1, 2$ , in this limit.

Near zero

$$\Lambda_j = 1 \pm \frac{\sqrt{3}\xi}{6}\sqrt{d_j} + O(\xi^2), \quad \xi \rightarrow 0. \quad (4.12)$$

In order that the correct sign in front of the above square root is chosen (so that  $|\Lambda_{1,2}| \leq 1$ ), it is necessary to analyse the behaviour of  $d_j$ ,  $j = 1, 2$  in (4.9) for  $\alpha > 0$  and  $0 < V_* \leq C_R(m/\mu_2)^{1/2}$ .

### The constants $d_{1,2}$

Here we show that  $d_{1,2}$  do not belong to the negative real axis in the complex plane. Otherwise

$$1 + \frac{\xi^2}{12}|d_j| > 1,$$

and then higher order terms would be needed in (4.12) to determine if  $|\Lambda_{1,2}| \leq 1$  as  $\xi \rightarrow 0$ . The proposition below is proved for  $d_1$  and the result extends to  $d_2$ .

**Proposition 2** *For  $\alpha > 0$  and  $0 < V_* \leq C_R(m/\mu_2)^{1/2}$ , we have  $d_1 \in \mathbb{C} \setminus \mathbb{R}_-$ .*

*Proof.* We begin by assuming on the contrary that  $d_1$  is negative, which is equivalent to the inequality

$$3(4\alpha - 1) - 16V_*^2 < 4\sqrt{4V_*^4 + 3(\alpha - 1)(3\alpha - 4V_*^2)} \quad (4.13)$$

with the assumption that the term under the square root in the right-hand side is positive. This gives rise to the cases:

a)

$$3(4\alpha - 1) - 16V_*^2 > 0,$$

together with

$$(3(4\alpha - 1) - 16V_*^2)^2 < 16(4V_*^4 + 3(\alpha - 1)(3\alpha - 4V_*^2))$$

or

b)

$$3(4\alpha - 1) - 16V_*^2 < 0 \quad \text{and} \quad 4V_*^4 + 3(\alpha - 1)(3\alpha - 4V_*^2) > 0.$$

*The Case a).* One can obtain the inequality

$$V_*^4 - \frac{2\alpha + 1}{2}V_*^2 + \frac{3}{8}\left(\alpha + \frac{1}{8}\right) < 0 .$$

The quadratic function of  $V_*^2$ , in the left-hand side, has the zeros

$$v_{1,2}^2 = \frac{3}{8}, \frac{1}{8} + \alpha ,$$

which for  $\alpha > 0$ , are both positive. Then (4.13) is only valid if  $V_*^2 \in (v_1^2, v_2^2)$  for  $\alpha \geq 1/4$  or  $V_*^2 \in (v_2^2, v_1^2)$  for  $\alpha < 1/4$ . We now show  $V_*^2$  lies outside these intervals for  $\alpha > 0$ .

By Proposition 1,

$$\max\{V_*^2\} = g(\alpha) \leq v_1^2 , \quad \text{when} \quad \alpha \geq 1/4 , \quad (4.14)$$

where  $g(\alpha)$  is given in (2.2).

For  $\alpha < 1/4$ , owing again to Proposition 1,

$$\frac{dg}{d\alpha}(\alpha) < \frac{3}{4} , \quad \text{for} \quad \alpha > 0 , \quad g(0) < \frac{1}{8} , \quad \text{and} \quad g(1/4) = \frac{3}{8}\left(1 - \frac{\sqrt{3}}{3}\right) < \frac{3}{8} .$$

Thus

$$\max\{V_*^2\} = g(\alpha) < v_2^2 , \quad \text{when} \quad 0 < \alpha < 1/4 .$$

This inequality with (4.14) shows that (4.13) is not valid for  $V_* \in (0, C_R\sqrt{m/\mu_2}]$  and  $\alpha > 0$  for case *a*) above.

*The Case b).* The second inequality of this case can be rewritten as

$$V_*^4 + 3(1 - \alpha)V_*^2 - \frac{9\alpha(1 - \alpha)}{4} > 0 , \quad (4.15)$$

where now the quadratic function on the left-hand side has zeros

$$w_{\pm}^2 = \frac{3}{2}[\alpha - 1 \pm \sqrt{1 - \alpha}] .$$

When  $\alpha \geq 1$  the inequality (4.15) is satisfied (since the zeros of the left-hand side are complex), and it remains to show that the inequalities

$$V_*^2 \leq \frac{C_R^2 m}{\mu_2} \quad \text{and} \quad V_*^2 > \frac{3(4\alpha - 1)}{16} , \quad (4.16)$$

do not hold. These lead to

$$\frac{3(4\alpha - 1)}{16} < g(\alpha) , \quad \text{or} \quad \sqrt{3\alpha^2 + (\alpha - 1)^2} < \frac{7}{4} - \alpha ,$$

where the definition of  $g(\alpha)$  in (2.2) has been used. From the above inequalities, we have a contradiction to (4.16) for  $\alpha \geq 7/4$ . Assume  $1 \leq \alpha < 7/4$ , then the last inequality leads to

$$\alpha^2 + \frac{1}{2}\alpha - \frac{11}{16} < 0 .$$

This is valid for  $\alpha \in (0, (-1/2 + \sqrt{3})/2)$ . Hence (4.13) does not hold.

When  $\alpha < 1$ , for (4.15) to be satisfied we put

$$V_*^2 > w_+^2 = \frac{3}{2}[\alpha - 1 + \sqrt{1 - \alpha}]$$

where

$$V_*^2 \leq \frac{C_R^2 m}{\mu_2} , \quad \text{and} \quad V_*^2 > \frac{3(4\alpha - 1)}{16} .$$

Here, as before, the last two inequalities are valid if  $0 < \alpha < (-1/2 + \sqrt{3})/2$ . It remains to check that

$$V_*^2 > w_+^2 = \frac{3}{2}[\alpha - 1 + \sqrt{1 - \alpha}] \quad \text{and} \quad V_*^2 \leq \frac{C_R^2 m}{\mu_2}. \quad (4.17)$$

Both of these yield the inequality

$$\alpha^2(\alpha^2 + \alpha - \frac{7}{4}) > 0.$$

This is valid for  $\alpha > -1/2 + \sqrt{2}$  and, since we have assumed that  $0 < \alpha < (-1/2 + \sqrt{3})/2$ , we have a contradiction to (4.17). Therefore, (4.13) is not valid for  $V_* \in (0, C_R(m/\mu_2)^{1/2}]$  and  $\alpha > 0$  in case b) above.  $\square$

#### 4.3.1 Asymptotes of $L(\xi)$

Here, we obtain the asymptotics of  $L(\xi)$  for  $\xi \rightarrow 0$ .

**Proposition 3** *For  $\xi \rightarrow 0$ , we have*

$$L(\xi) \sim L_0 \frac{1}{\sqrt{(\varepsilon + i\xi)(\varepsilon - i\xi)}} + O(|\xi|), \quad \varepsilon \rightarrow +0, \quad (4.18)$$

where

$$L_0 = \frac{3\sqrt{d_1 d_2}(B_2\sqrt{d_1} + B_1\sqrt{d_2})}{2\sqrt{3}(3 - 8V_*^2)(2V_*^2 - 3\alpha)(V_*^4 - \frac{1}{2}(2\alpha + 1)V_*^2 + \frac{3\alpha}{8})}, \quad (4.19)$$

and

$$B_j = \frac{1}{2} \left[ \frac{1}{6} (V_*^2 - (-1)^j M_0)^2 - V_*^2 \left( \frac{3V_*^2}{2} + 1 \right) - \frac{3\alpha}{2} \left( \alpha - \frac{1}{2} - 2V_*^2 \right) \right], \quad j = 1, 2.$$

*Proof.* Using (4.8), for  $\xi \rightarrow 0$ :

$$z_2 - z_1 = \frac{M_0 \xi^2}{3} + O(\xi^4), \quad (4.20)$$

and

$$F(z_j) = B_j \xi^4 + O(\xi^6), \quad j = 1, 2,$$

together with (4.6), (4.9), (4.10), (4.20) gives (4.18), where

$$L_0 = \frac{M_0 \sqrt{d_1 d_2}}{2\sqrt{3}(B_2\sqrt{d_1} - B_1\sqrt{d_2})}.$$

Multiplying the numerator and the denominator by  $B_2\sqrt{d_1} + B_1\sqrt{d_2}$ , we arrive at (4.19).  $\square$

It is shown in Appendix I that  $L_0$  is positive for  $\alpha > 0$ , and  $V \leq C_R$ .

## 5 Roots and poles of the kernel function $L(\xi)$

Having obtained the expression for the kernel function  $L(\xi)$ , we can now derive expressions for the dispersion relations of the inhomogeneous lattice. We also show that these relations can be used to predict the behaviour of the argument of the function  $L$ , which is needed in the computation of the energy release rate for the propagating crack in section 7. Let  $m = 1$  and let

$$p = 3r(\Lambda_1^*)r(\Lambda_2^*)\sqrt{z_1^2 - 1}\sqrt{z_2^2 - 1}$$

and

$$q = \frac{r(\Lambda_1^*)F(z_2)\sqrt{z_1^2 - 1} - r(\Lambda_2^*)F(z_1)\sqrt{z_2^2 - 1}}{z_2 - z_1} \quad (5.1)$$

so that in (4.6)

$$L(\xi) = \frac{p}{q}.$$

We now investigate the zeros of  $p$  and  $q$  of the above expression. This is carried out by setting  $\varepsilon = 0$  and  $\Omega = \xi V$ , then solving the equations  $p = 0$  and  $q = 0$  for  $\Omega$ .

The roots of the equation  $p = 0$  are given by:

$$\Omega_1^{(N)}(\xi) = \sqrt{6\mu_2} |\cos(\xi/4)|, \quad (5.2)$$

$$\Omega_2^{(N)}(\xi) = [2\mu_2 \sin^2(\xi/4) + 4\mu_1 \sin^2(\xi/2)]^{1/2}, \quad (5.3)$$

$$\Omega_3^{(N)}(\xi) = \sqrt{6\mu_2} |\sin(\xi/4)|, \quad (5.4)$$

$$\Omega_4^{(N)}(\xi) = [2\mu_2 \cos^2(\xi/4) + 4\mu_1 \sin^2(\xi/2)]^{1/2}. \quad (5.5)$$

Next we obtain the roots of the equation  $q = 0$ . This equation, after multiplication by

$$r(\Lambda_2^*)F(z_2)\sqrt{z_1^2 - 1} + r(\Lambda_1^*)F(z_1)\sqrt{z_2^2 - 1},$$

leads to

$$\frac{F(z_2)^2(z_1^2 - 1) - F(z_1)^2(z_2^2 - 1)}{(z_2 - z_1)} = 0. \quad (5.6)$$

Solutions of this extended equation are then (5.4), (5.5) and

$$\Omega_1^{(D)}(\xi) = \sqrt{2\mu_1 + \mu_2 - \sqrt{3\mu_1^2 + (\mu_1 - \mu_2)^2} |\sin(\xi/2)|}, \quad (5.7)$$

$$\Omega_2^{(D)}(\xi) = \sqrt{6\mu_1} |\sin(\xi/2)|, \quad (5.8)$$

$$\Omega_3^{(D)}(\xi) = \sqrt{2\mu_1 + \mu_2 + \sqrt{3\mu_1^2 + (\mu_1 - \mu_2)^2} |\sin(\xi/2)|}, \quad (5.9)$$

and it remains to determine which of the roots of (5.6) are those of (5.1). Note that for each dispersion relation  $\Omega(\xi + 4\pi) = \Omega(\xi)$ .

Functions (5.4) and (5.5) are roots of equation (5.1) and are in fact removable singularities of  $L(\xi)$ .

The choice of  $\alpha$  and  $\xi$  determines when (5.7)–(5.9) are solutions of  $q = 0$ . Here, we present the results for the case  $\alpha = 1$  and give the description of the behaviour of the argument of  $L$ . The function  $\Omega_1^{(D)}$  is a solution of (5.1). When

$$0.6667 \leq \xi/\pi \leq 1.3333 \quad \text{and} \quad 2.6667 \leq \xi/\pi \leq 3.3333, \quad (5.10)$$

we have  $\Omega_2^{(D)}$  is a solution of  $q = 0$ . For  $\xi/\pi$  satisfying

$$0.7614 \leq \xi/\pi \leq 1.2386 \quad \text{and} \quad 2.7614 \leq \xi/\pi \leq 3.2386, \quad (5.11)$$

$\Omega_3^{(D)}$  is a solution of  $q = 0$ . The inequalities (5.10) and (5.11) and their derivations are discussed in the Appendix II.

In Figure 3(a) we plot the dispersion relations (5.2)–(5.5) and (5.7)–(5.9), as functions of the wavenumber  $\xi$ , for  $\mu_1 = \mu_2 = 1$ . Included in this figure is the ray  $\Omega = V\xi$  corresponding to the speed  $V = 0.4504$ . By comparison with the diagram of  $\arg(L(\xi))$  in Figure 3(b), we see each intersection of the ray  $\xi V$  with the dispersion curves corresponds to a jump in  $\arg(L(\xi))$ .

At approximately  $\xi = \pi$ , we have an additional jump in  $\arg(L(\xi))$ . This is a result of the behaviour of the factor  $z_2 - z_1$  contained in  $L$  (see (4.6) and (3.4)). This factor, as shown in Figure 3(c), is either real or purely imaginary. As we approach  $\xi = \pi$ , this factor goes moves from the negative imaginary axis in the complex plane, to the positive real axis (note that  $z_2 - z_1$  is the radical function of (3.5) where the positive square root is taken). The corresponding effect is a jump in  $\arg(L(\xi))$  of  $\pi/2$ .

For a lower crack speed,  $V = 0.21395$ , we present the dispersion diagram along with the ray  $\xi V$  in Figure 4(a). On the corresponding picture for  $\arg(L(\xi))$  in Figure 4(b), we see this function jumps when the ray intersects the dispersion curves. In particular, the ray  $\xi V$  intersects the curve corresponding to  $\Omega_3^{(D)}$  in the second region of (5.11), which again results in a change in the value of  $\arg(L(\xi))$ . Also, in Figure 4(c), at approximately,  $\xi = 3.4\pi$ , we observe that the factor  $z_2 - z_1$  moves from the positive real axis to the positive imaginary axis. Again, the result we see is a jump of  $\pi/2$  in  $\arg(L(\xi))$  at this point.

Finally, for  $\mu_1 = 1$  and  $\mu_2 = 10$ , ( $\alpha = 0.1$ ),  $V = 0.799076$  we present the dispersion relations, the plot of  $\arg(L(\xi))$  and the imaginary part of the factor  $z_2 - z_1$ , in Figure 5(a)–(c). Comparing with Figure 3, we see the distance between the dispersion curves along with their height has increased, which can lead to greater absolute value of the area under the curve traced by the argument of  $L$ .

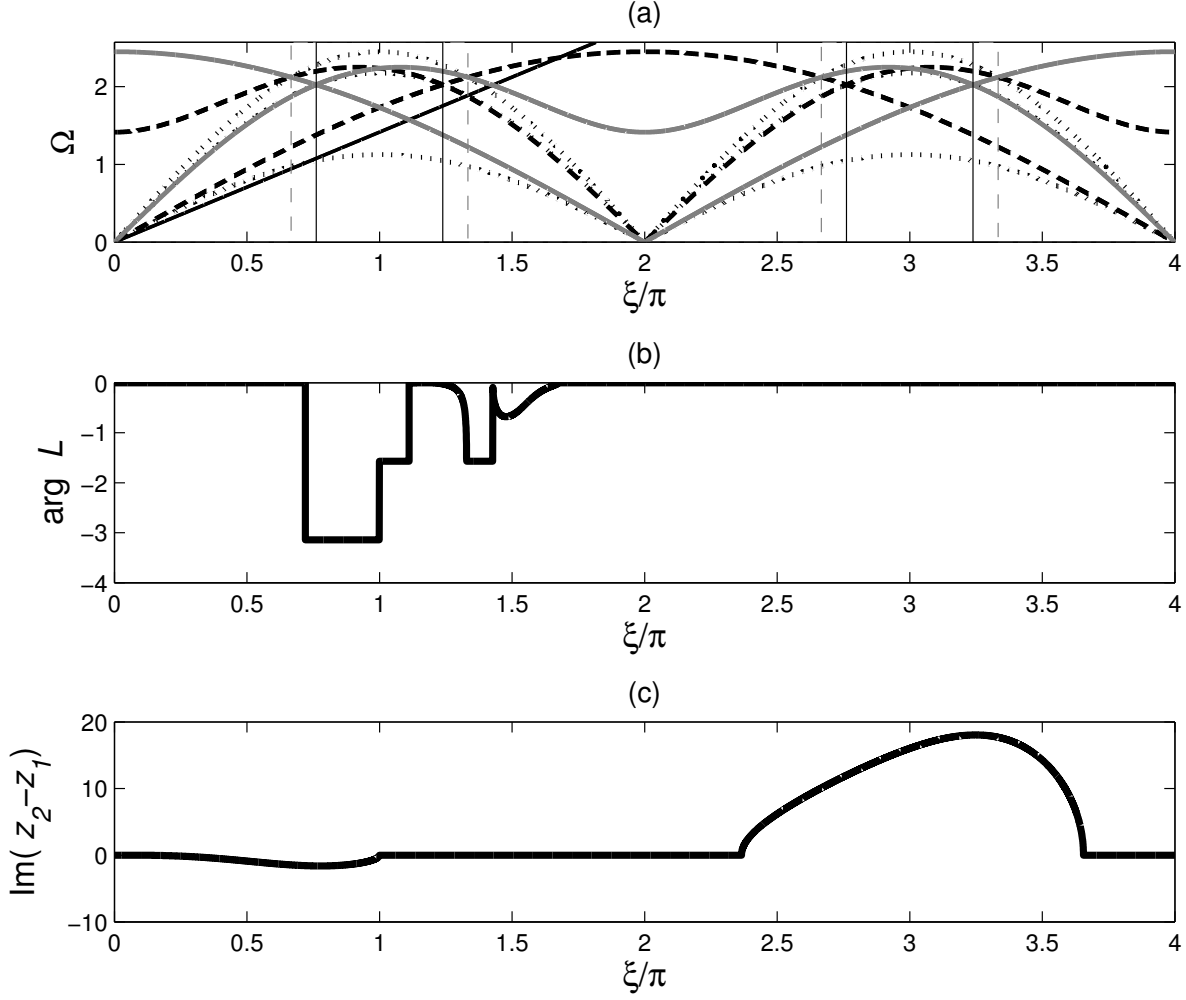


Figure 3: For  $\mu_1 = \mu_2 = 1$ ,  $\alpha = 1$ , figure (a) shows the dispersion relations (5.2)–(5.5) and (5.7)–(5.9), along with the ray  $\xi V$  for  $V = 0.4504$ . The roots of  $L$  are given by the solid curves, poles are shown by curves with the small dashes and the removable singularities are given by the dashed curves. The regions given in (5.10) and (5.11) where  $\Omega_2^{(D)}$  and  $\Omega_3^{(D)}$  are roots of  $q = 0$  are marked by the dashed and solid vertical lines. For comparison, we give the plot of (b)  $\arg(L(\xi))$ , and (c) the imaginary part of the factor  $z_2 - z_1$  contained in the representation (4.6) of  $L$ .

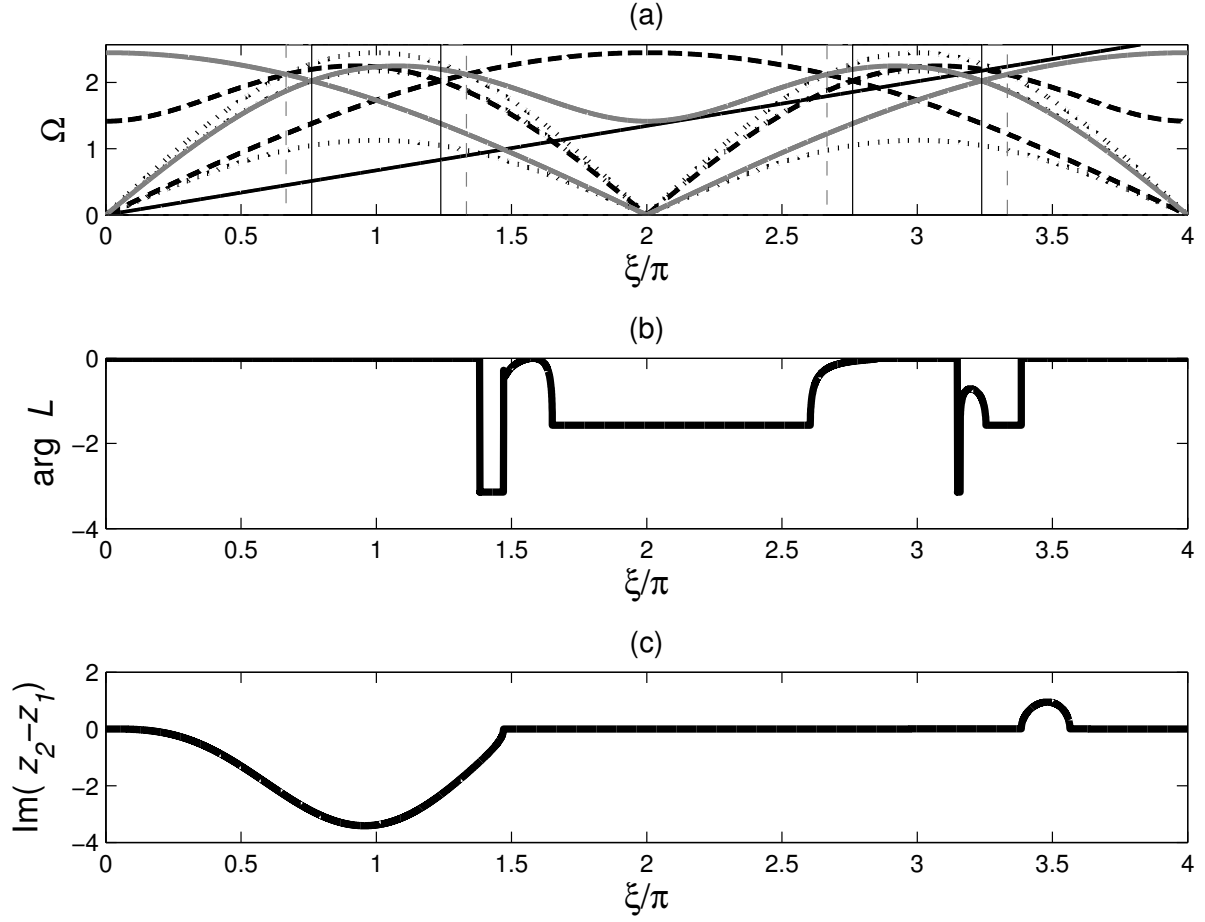


Figure 4: For  $\mu_1 = \mu_2 = 1$ ,  $\alpha = 1$ , in figure (a) we show the dispersion relations (5.2)–(5.5) and (5.7)–(5.9), along with the ray  $\xi V$  for  $V = 0.21395$ . The description of the curves in the dispersion diagram is the same as in Figure 3. We again give the plot of (b)  $\arg(L(\xi))$  and (c) the function  $\text{Im}(z_2 - z_1)$ , for the purpose of comparison.

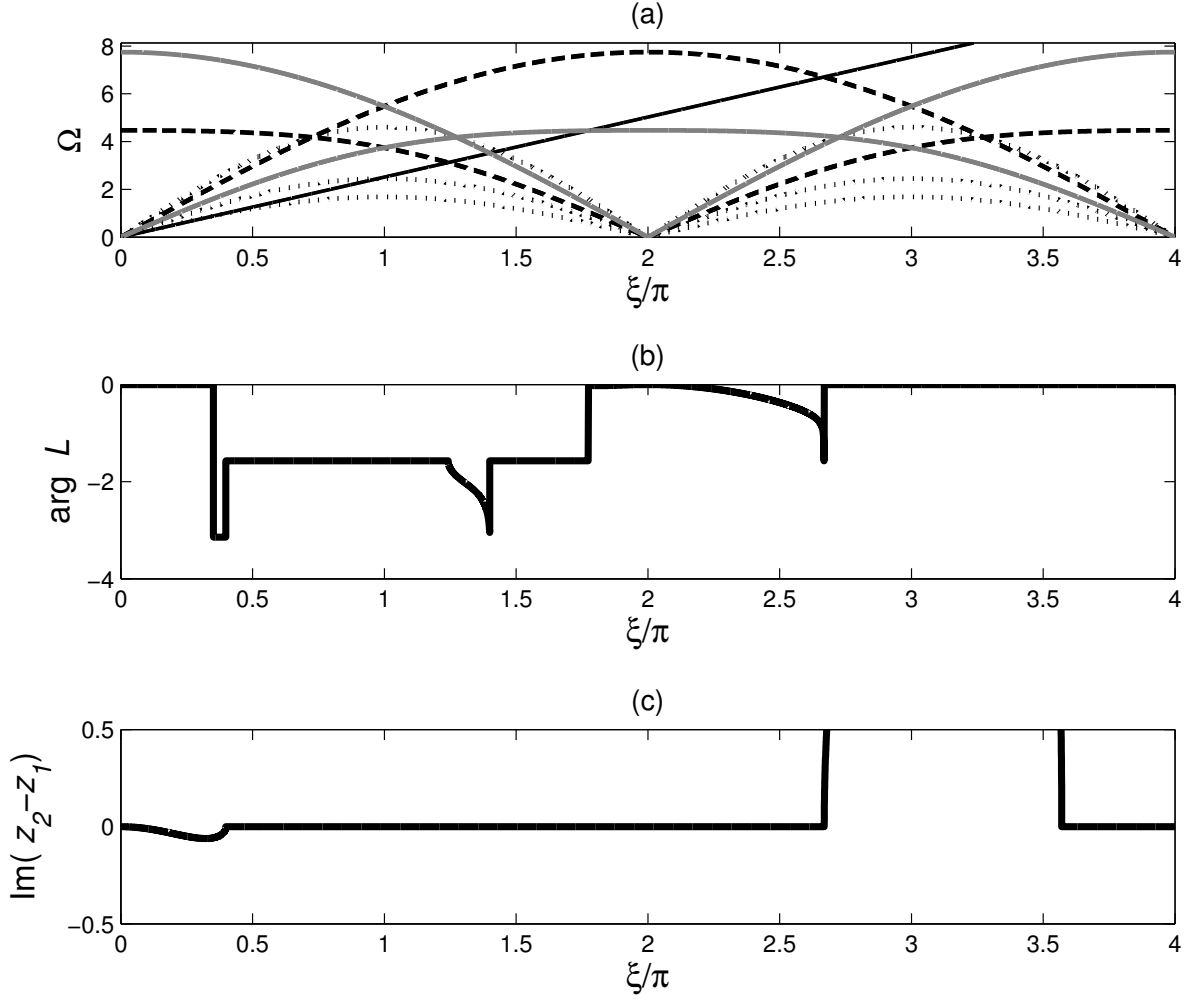


Figure 5: (a) For  $\mu_1 = 1$ ,  $\mu_2 = 10$ ,  $\alpha = 0.1$ , we plot the dispersion relations (5.2)–(5.5) and (5.7)–(5.9), along with the ray  $\xi V$  for  $V = 0.79976$ . The description of the dispersion curves is given in Figure 3. The plots of (b)  $\arg(L(\xi))$  and (c)  $\text{Im}(z_2 - z_1)$  are also presented.

## 6 Solution of the Wiener-Hopf equation

### 6.1 Factorisation of the Wiener-Hopf equation (4.5)

Here, we use the solution presented in [Slepyan (2002)] and extend it to the situation when the bonds within the lattice have a contrast in stiffness in the principal lattice directions. We define the class  $\mathcal{J}$  as the set of complex valued functions  $f : \mathbb{R} \rightarrow \mathbb{C}$  satisfying

$$\operatorname{Re}(f(\xi)) = \operatorname{Re}(f(-\xi)) , \quad \operatorname{Im}(f(\xi)) = -\operatorname{Im}(f(-\xi)) .$$

For  $\varepsilon > 0$ , the kernel  $L \in \mathcal{J}$  and satisfies

$$\begin{aligned} \operatorname{Ind}(L(\xi)) &= \frac{1}{2\pi} [\arg(L(+\infty)) - \arg(L(-\infty))] = 0 , \\ \arg(L(\xi)) &= -\arg(L(-\xi)) \quad \text{and} \quad L(\pm\infty) = 1 , \end{aligned} \tag{6.1}$$

where  $\operatorname{Ind}(L(\xi))$  represents the number of times the contour traced by  $L(\xi)$  in the complex plane winds around the origin. The proof of these properties are given in Appendix III.

Then, the above conditions allow  $L(\xi)$  to be factorised in the form

$$L = L_+ L_- ,$$

where

$$L_{\pm}(\varepsilon + i\xi V, \xi) = \exp \left( \pm \frac{1}{2\pi i} \int_{-\infty}^{\infty} \frac{\ln L(\varepsilon + isV, s)}{s - \xi} ds \right) \tag{6.2}$$

with  $\varepsilon \rightarrow +0$ ,  $\operatorname{Im} \xi > 0$  for  $L_+$  and  $\operatorname{Im} \xi < 0$  for  $L_-$ .

The function  $L_+$  ( $L_-$ ) is an analytic function of  $\xi$  in the upper (lower) half-plane. The introduction of the small positive parameter  $\varepsilon$  into  $L$ , shifts its zeros and poles (located on the real axis) into the upper or lower half of the complex plane. Following this shift, the dispersion curves, discussed in section 5, can be then used to identify in which half plane each root and pole is located (see Slepyan [Slepyan (2002), Chapter 2]).

Suppose  $\xi_z$  and  $\xi_p$  are wavenumbers which correspond to the intersection of  $\Omega = \xi V$  with the zeros and poles of  $L$ , respectively (see (5.2)–(5.5) and (5.7)–(5.9)), on the dispersion diagram. Also at these intersection points, let  $V < V_g$ , where  $V_g = d\Omega/d\xi$  is the group velocity. Then, in this case  $\xi_z$  and  $\xi_p$  will be located in the lower half plane after the introduction of  $\varepsilon$  in  $L$ . Similarly, if  $V > V_g$  then  $\xi_z$  and  $\xi_p$  are shifted into the upper half of the complex plane (see [Slepyan (2002), Section 3.3.3]). From the definition (6.2), it follows that  $L_+$  ( $L_-$ ) contains all singular and zero points of  $L$  which are located in the lower (upper) half of the complex plane for  $\varepsilon > 0$ .

Using (6.1), equation (4.5) can then be written as

$$L_+ \mathcal{S}_+ + \frac{\mathcal{S}_-}{L_-} = \left( \frac{1}{L_-} - L_+ \right) \phi^F , \tag{6.3}$$

which is the same as (12.58) of [Slepyan (2002)].

Here, the left-hand side of (6.3) is the sum of two analytic functions, one analytic in the upper half of the complex plane, the other analytic in the lower half of the complex plane and in order to solve the problem, we must separate the terms in the right-hand side in the same way. This is carried out by introducing the load  $\phi$  in such a way that it allows for this additive split. In Appendix IV, an outline for this procedure is presented for the case when the load  $\phi$  is chosen so that the right-hand side can be represented as a linear combination of Dirac delta functions.

In what follows, we will consider the situation when the load applied along the crack faces which generates term of the form  $\mathcal{C}\delta(\xi)$ , in the right-hand side of (6.3) (see Appendix IV for the derivation). Here,  $\mathcal{C}$  is a constant which represents the intensity of the load. Then  $\mathcal{S}_+$  and  $\mathcal{S}_-$  have the form

$$\mathcal{S}_+ = \frac{\mathcal{C}}{L_+(\xi)(\varepsilon - i\xi)} , \quad \mathcal{S}_- = \frac{L_-(\xi)\mathcal{C}}{\varepsilon + i\xi} , \quad \varepsilon \rightarrow +0 , \tag{6.4}$$



## 7 Energy release rate ratio

Here, we investigate the dependence of energy release rate ratio [Slepyan (2002)] on the stiffness contrast parameter  $\alpha$ . This is defined as

$$\frac{G_0}{G} = \exp \left( \frac{2}{\pi} \int_0^\infty \frac{\arg(L(\varepsilon + isV, s))}{s} ds \right), \quad \varepsilon \rightarrow +0, \quad (7.1)$$

where  $G_0$  is the local energy release rate for the semi-infinite crack propagating through the lattice with speed  $V$  for sub-Rayleigh wave speed and  $G$  is global energy release rate for the crack propagating through the corresponding homogenised medium. This ratio describes the dissipation of energy created by breaking bonds at the crack front.

Next we show (7.1) can be obtained from (6.4). However, we note that the derivation of (7.1) does not depend on the solution of the Wiener-Hopf equation in the previous section. The definitions of  $G$  and  $G_0$  follow [Slepyan (2002), Chapter 12] as the energy release rates globally and locally respectively. In particular, as in [Slepyan (2002)],  $G$  can be defined as a limit

$$G = \lim_{k \rightarrow 0} \varepsilon^2 \mathcal{S}_-(ik) \mathcal{S}_+(ik),$$

and the local energy release rate is given as

$$G_0 = \lim_{k \rightarrow +\infty} \varepsilon^2 \mathcal{S}_-(ik) \mathcal{S}_+(ik).$$

The global energy release rate  $G$  follows from the asymptotes of  $\mathcal{S}_\pm$  as  $\xi \rightarrow 0$ . The asymptotes of  $L_\pm$  are

$$\begin{aligned} L_+(\varepsilon + i\xi V, \xi) &\sim \frac{\sqrt{L_0}}{\sqrt{\varepsilon - i\xi}} \exp \left( \frac{1}{\pi} \int_0^\infty \frac{\arg(L(\varepsilon + isV, s))}{s} ds \right), \\ L_-(\varepsilon + i\xi V, \xi) &\sim \frac{\sqrt{L_0}}{\sqrt{\varepsilon + i\xi}} \exp \left( -\frac{1}{\pi} \int_0^\infty \frac{\arg(L(\varepsilon + isV, s))}{s} ds \right), \end{aligned} \quad (7.2)$$

for  $\varepsilon \rightarrow +0$ , and their derivations are found in Appendix V.

Then, owing to (6.4) and (7.2),

$$\begin{aligned} \mathcal{S}_+ &\sim \frac{\mathcal{C}}{\sqrt{L_0} \sqrt{\varepsilon - i\xi}} \exp \left( -\frac{1}{\pi} \int_0^\infty \frac{\arg(L(\varepsilon + isV, s))}{s} ds \right), \\ \mathcal{S}_- &\sim \frac{\sqrt{L_0} \mathcal{C}}{(\varepsilon + i\xi)^{3/2}} \exp \left( -\frac{1}{\pi} \int_0^\infty \frac{\arg(L(\varepsilon + isV, s))}{s} ds \right), \end{aligned} \quad (7.3)$$

where  $\xi \rightarrow 0$ ,  $\varepsilon \rightarrow +0$ , and then

$$G = \mathcal{C}^2 \exp \left( -\frac{2}{\pi} \int_0^\infty \frac{\arg(L(\varepsilon + isV, s))}{s} ds \right), \quad \varepsilon \rightarrow +0. \quad (7.4)$$

The local energy release rate is then given by the asymptotes of  $\mathcal{S}_\pm$  when  $\xi \rightarrow \infty$ . As a result of (6.1) and (6.2),  $L_\pm \rightarrow 1$  as  $\xi \rightarrow \infty$ . In the same limit we have

$$\mathcal{S}_+ \sim \frac{\mathcal{C}}{\varepsilon - i\xi}, \quad \mathcal{S}_- \sim \frac{\mathcal{C}}{\varepsilon + i\xi}, \quad \xi \rightarrow \infty, \varepsilon \rightarrow +0,$$

and so  $G_0 = \mathcal{C}^2$ . Then this and (7.4) imply (7.1).

### 7.1 Sensitivity of the energy release rate ratio to the stiffness contrast

In this section, we set  $m = \mu_1 = 1$ , so that  $\alpha = 1/\mu_2$ , and we investigate the behaviour of the energy release rate ratio (7.1) as a function of crack speed, when the stiffness ratio is increased (which corresponds to the decrease in the stiffness of the inclined bars). The critical crack speed  $C_R(\alpha)$ , in this example, has the form (see (2.1)):

$$C_R(\alpha) \Big|_{m=1, \mu_1=1} = \frac{1}{2\alpha^{1/2}} \sqrt{2\alpha + 1 - \sqrt{3\alpha^2 + (\alpha - 1)^2}}. \quad (7.5)$$

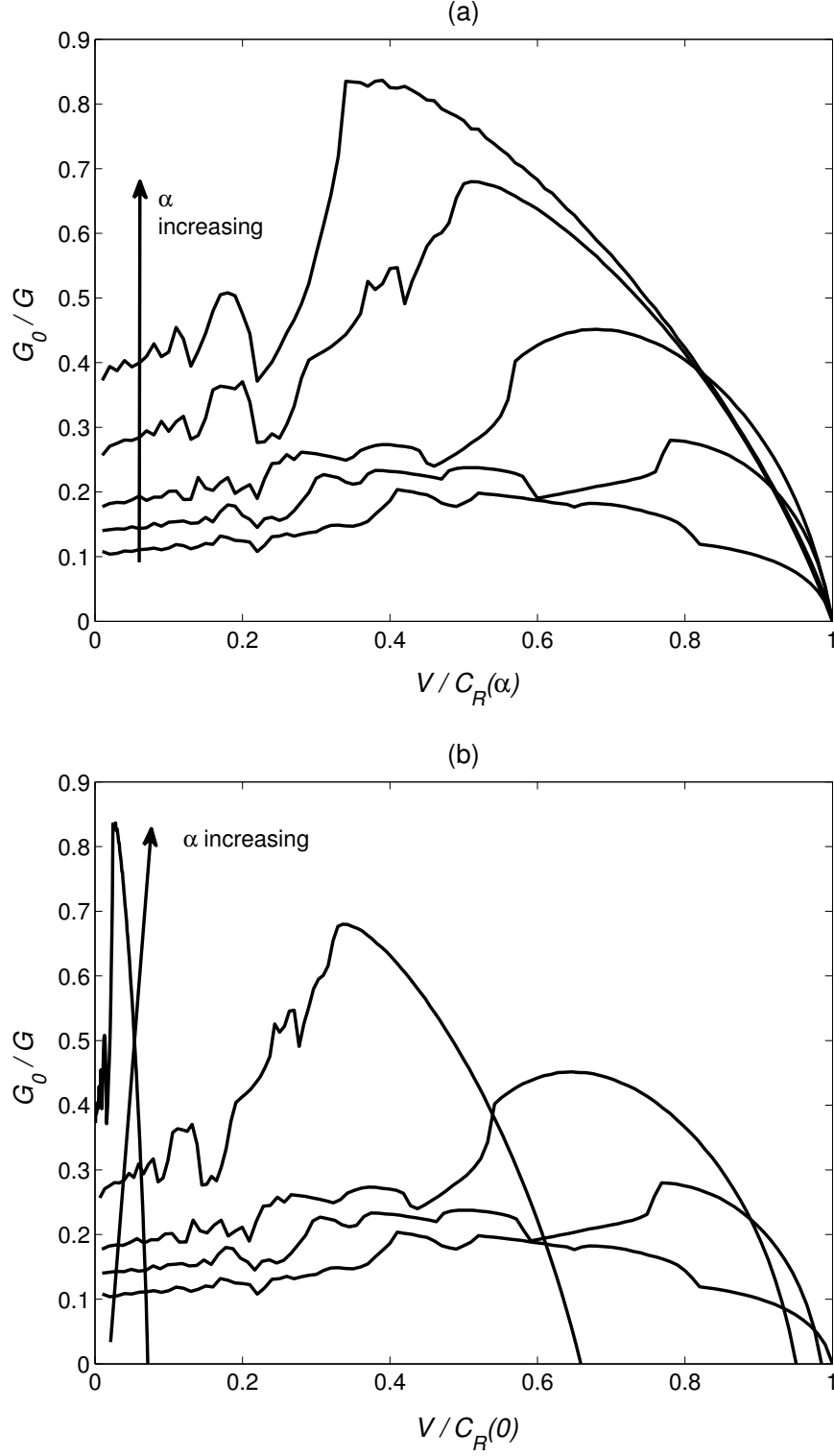


Figure 6: (a): The energy release rate ratio as a function of the normalised speed  $V/C_R(\alpha)$ , based on formula (7.1). (b) The ratio  $G_0/G$  as a function of the crack speed normalised by the supremum of  $C_R(\alpha)$  over  $\alpha > 0$  ( $C_R(0) = \sqrt{3}/2$ ). We show the behaviour of this ratio for the stiffness contrasts  $\alpha = 0.05, 0.1, 0.2, 1$ , and  $100$ .

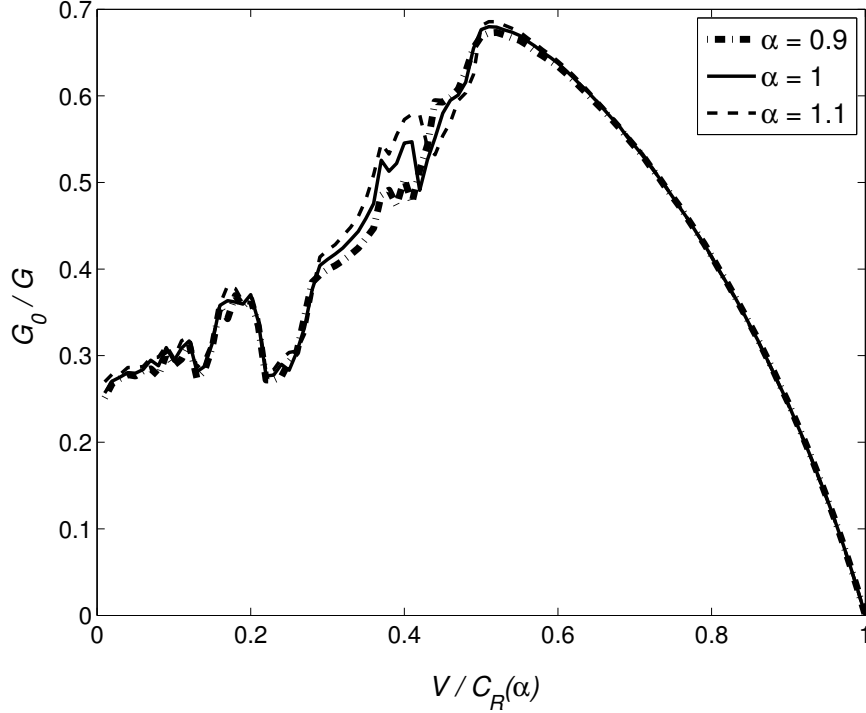


Figure 7: The energy release rate ratio as a function of the normalised speed  $V/C_R(\alpha)$ , computed using formula (7.1), for the values  $\alpha = 0.9, 1$  and  $1.1$ .

The lattice Rayleigh speed  $C_R(\alpha)$  is decreasing monotonically as  $\alpha$  increases. The upper bound of this function is  $C_R(0) = \sqrt{3}/2$ , (when the inclined bars are rigid) and for  $\alpha$  tending to infinity (the inclined bars are becoming much more softer compared to the horizontal bars) the speed  $C_R(\alpha)$  tends to zero. In Figure 6(a), we plot the energy release rate ratio as a function of normalised crack speed  $V/C_R(\alpha)$ , for  $\alpha = 0.05, 0.1, 0.2, 1, 100$ . The crack, for low speeds, does not propagate steadily. The intrinsic feature of the model discussed here is that the crack propagates uniformly with speed  $V$ . If this assumption is not satisfied then the model does not describe accurately the propagation of the crack, which is depicted by the non-smooth part of the curves on Figure 6(a), e.g. for approximately  $V/C_R(\alpha) < 0.5$  when  $\alpha = 1$ . This region of instability is caused by the highly oscillatory behaviour of  $\arg(L(\xi))$  for low crack speeds, in (7.1), as observed in section 5. From Figure 6(a), we see the percentage of speeds less than  $C_R(\alpha)$ , where this region is located, is decreasing as  $\alpha$  is increasing.

Contained in Figure 6(b), is the plot of the energy release rate ratio against the crack speed which has been normalised by  $C_R(0) = \sqrt{3}/2$ . For  $\alpha \geq 0.05$  the ratio  $G_0/G$  tends to zero as we approach critical speed  $C_R(\alpha)$  predicted by (7.5). For  $\alpha > 0.1$ , in the region of instability, the ratio  $G_0/G$  increases until it reaches a speed where there is a global maximum. For speeds greater than this, we observe the ratio follows a smooth curve as it decreases to zero at the critical Rayleigh speed (7.5). In this region, this behaviour shows that the model describes the steady propagation of the semi-infinite crack through the inhomogeneous lattice.

In [Mishuris, et al. (2009b)], the dynamic problem for the propagation of a crack situated in a square-cell lattice, whose rows contain particles of contrasting mass, is discussed. The sensitivity to the contrast in mass, of the ratio of the local energy release rate  $G_0$  (for the lattice) to the global energy release rate  $G$  (for the corresponding homogenised material) was also investigated. It was seen the values of  $G_0/G$ , for high crack speeds, increased monotonically as the contrast in mass was reduced. Here, as shown in Figures 6(a), (b) and 7, we do not have any monotonicity in the behaviour of  $G_0/G$  for different  $\alpha$ . For example, in Figure 6(a), the curve for  $\alpha = 0.2$  intersects those for  $\alpha = 1, 100$  at approximately  $V/C_R(\alpha) = 0.83$  (where we are in the region of stability for all these curves). For speeds higher than this value, the ratio of  $G_0/G$  for  $\alpha = 0.2$  is greater than that for  $\alpha = 1$  and  $\alpha = 100$ . A similar example can be seen for the curve corresponding to  $\alpha = 0.1$ .

It was also seen in [Mishuris, et al. (2009b)], for low crack speeds corresponding to the instability region of the model, the values of  $G_0/G$  were not monotonic as a function of the mass contrast parameter. A similar

feature is also observed here for low crack speeds as the stiffness contrast parameter  $\alpha$  is varied. In Figure 7, we plot the energy release rate ratio for  $\alpha = 0.9, 1$  and  $1.1$ . For speeds  $V/C_R(\alpha) < 0.5$  (the region of instability), there exists regions where all curves are intersecting one another and overlapping. For instance, when  $0.35 < V/C_R(\alpha) < 0.5$ , again there is no monotonicity in the behaviour of  $G_0/G$  as  $\alpha$  varies. We note that the critical speed in the scalar case [Mishuris, et al. (2009b)], was a material constant and did not depend on the contrast ratio.

## 8 Stress intensity factor in the homogenisation approximation

In this section, we derive the expression for the Mode I stress intensity factor for the semi-infinite crack in the case when the load  $\phi$  applied along the crack faces generates the term  $\mathcal{C}\delta(\xi)$  in the right-hand side of (6.3), with  $\mathcal{C}$  being the load intensity. The solution of this problem is given in (6.4).

Using the fact that the energy required to break the crack front bond  $G_0 = \mathcal{C}^2$  (see the previous section), we compute the inverse Fourier transform of  $\mathcal{S}_+$  in (7.3), so that to leading order

$$\mathcal{S}(\eta) \sim \sqrt{\frac{G_0}{L_0\pi\eta}} \exp\left(-\frac{1}{\pi} \int_0^\infty \frac{\arg(L(\varepsilon + isV, s))}{s} ds\right), \quad \text{for } \eta > 0 \quad (8.1)$$

which depends on  $\alpha$  and here  $L_0$  is given in Proposition 3. Here, the expression  $\mu_2\mathcal{S}(\eta)$  represents the tensile force in the inclined bonds ahead of the crack. Let the normal traction ahead of the crack be  $\sigma$ , then

$$\sigma \sim \mu_2 \sqrt{\frac{3G_0}{L_0\pi\eta}} \exp\left(-\frac{1}{\pi} \int_0^\infty \frac{\arg(L(\varepsilon + isV, s))}{s} ds\right). \quad (8.2)$$

The Mode I stress intensity factor  $K_I$ , in the far-field is defined by the formula

$$K_I = \lim_{\eta \rightarrow +0} \sqrt{2\pi\eta} \sigma. \quad (8.3)$$

On comparison of (8.2) and (8.3), we have the stress intensity factor  $K_I$  is

$$K_I(\alpha) = \mu_2 \sqrt{\frac{6G_0}{L_0}} \exp\left(-\frac{1}{\pi} \int_0^\infty \frac{\arg(L(\varepsilon + isV, s))}{s} ds\right). \quad (8.4)$$

Now, setting  $\mu_1 = 1$  and allowing  $\mu_2$  to vary, we investigate the behaviour of  $K_I$  as a function of  $V$  and  $\alpha$ . The expression for  $K_I/\sqrt{G_0}$  is given as a function of the normalised speed  $V/C_R(\alpha)$  in Figure 8(a) and as a function of the normalised speed  $V/C_R(0)$  in Figure 8(b) for  $\alpha = 0.05, 0.1, 0.2, 1, 100$  (where  $V \leq C_R(\alpha)$ , see (7.5)).

As discussed in the previous section, at low speeds the model presented here does not describe the propagation of the crack through the inhomogeneous lattice accurately. This is due to the highly oscillatory behaviour of the argument of  $L(\xi)$  and it leads to regions of instability, represented by the non-smooth behaviour in  $G_0/G$  for low speeds as seen in Figure 6. Since the expression  $K_I/\sqrt{G_0}$  contains the ratio  $\sqrt{G/G_0}$  (see (7.1) and (8.4)), we also see a similar behaviour in  $K_I/\sqrt{G_0}$  in Figure 8(a) and (b). For those speeds in this unstable region there is little physical significance of the results presented in the figures below. As we increase the speed of the crack, we leave the region of instability, and the stress intensity factor becomes a smooth function of the crack speed, and tends to a finite value for  $V$  tending to the Rayleigh speed  $C_R(\alpha)$  in (7.5), as shown in Figure 8(a). For  $\alpha < 1$ , in the vicinity of  $C_R(\alpha)$ ,  $K_I$  is a monotonically decreasing function for increasing  $V$ . When  $\alpha \geq 1$ , outside the instability region,  $K_I$  passes through a global minimum before the converging to a finite value at  $C_R(\alpha)$ . From the figure, we can see that overall the behaviour of the stress intensity factor is increasing as we decrease the stiffness contrast  $\alpha$ .

## 9 Conclusions

The paper has brought together analytical insight on a propagating semi-infinite fault in an elastic lattice with the computational experiments and physical interpretation of the fields in such a lattice structure. One of the

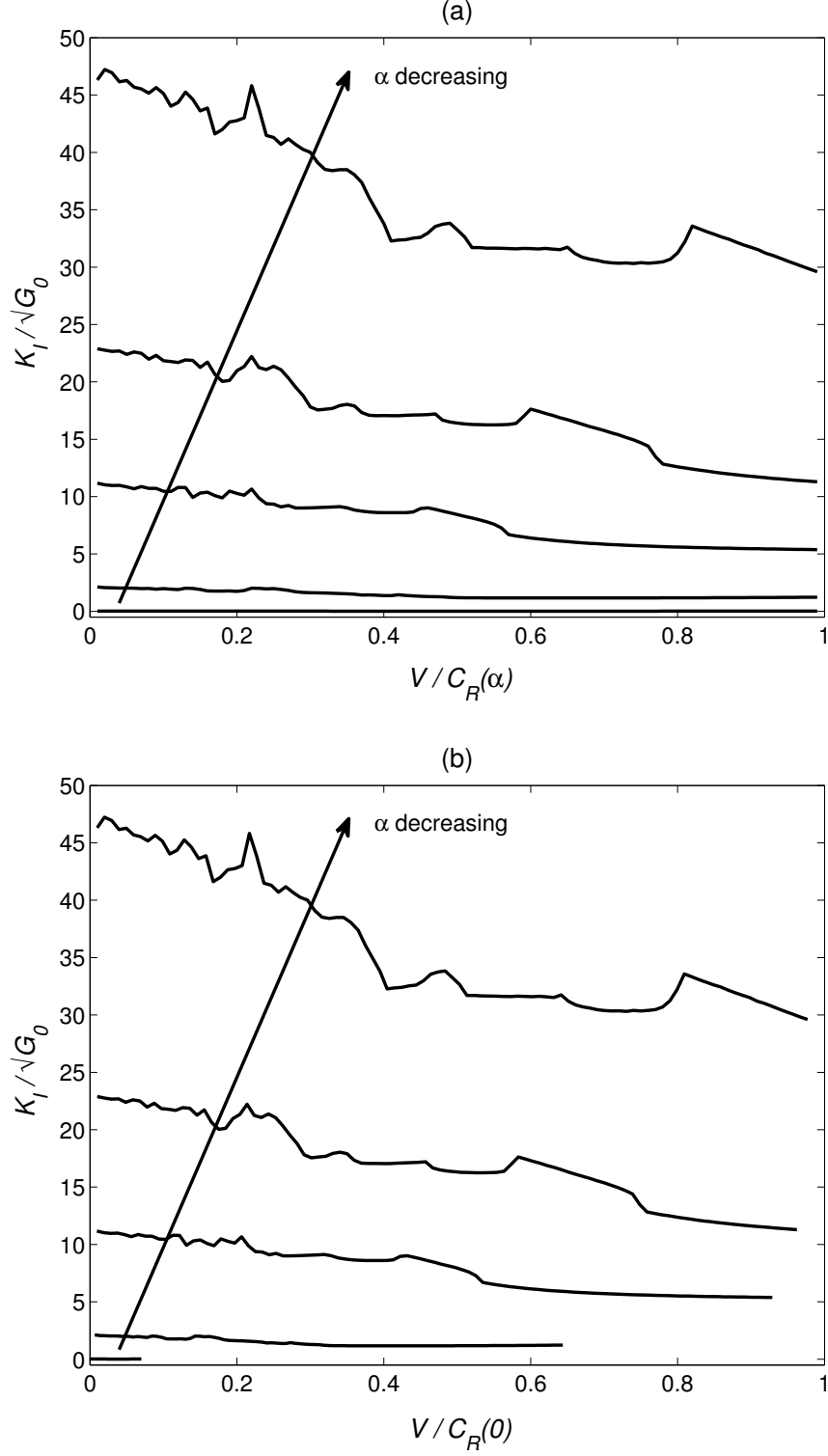


Figure 8: The normalised stress intensity factor  $K_I / \sqrt{G_0}$  as a function of (a) the normalised crack speed  $V / C_R(\alpha)$  and (b) the normalised crack speed  $V / C_R(0)$ , based on formula (8.1), for  $\alpha = 0.05, 0.1, 0.2, 1, 100$ . Here  $C_R(0) = \sqrt{3}/2$  is the supremum of (7.5) for  $\alpha > 0$ .

important issues discussed here is the crack stability for different regimes of the crack speed and different values of elastic parameters of the anisotropic lattice.

Although it appears that the analytical solution has a serious limitation due to the assumption of the steady crack propagation, it has been shown in [Mishuris, et al. (2009a)] that in the non-steady regime the averaging procedure appears to be viable. In this case, the averaged solution follows the prediction of the linear model constructed for the case of the steady crack propagation through the lattice.

It is also noted that the low-speed unsteady regime, predicted by the model, appears to be consistent with the results obtained by other approaches (see, for example, [Marder and Gross (1995)]), and it has a clear physical interpretation of an accelerating crack at the initial stage (low speed) of the crack advance.

In particular, the crack stability for different values of the lattice contrast is a challenging issue, which has been comprehensively addressed here.

**Acknowledgments.** M. J. Nieves would like to acknowledge the financial support of the U.K. Engineering and Physical Sciences Research Council through the research grant EP/H018514/1. Support through European grant FP7-PEOPLE-IAPP (PIAPP-GA-284544-PARM-2), held by G.S. Mishuris, is also gratefully acknowledged.

## References

- [Fineburg and Marder (1999)] Fineburg, J., Marder, M., 1999: Instability in dynamic fracture. *Physics Reports*, 313, 1–108.
- [Marder and Gross (1995)] Marder, M., Gross, S., 1995: Origin of crack tip instabilities. *J. Mech. Phys. Solids* 43, (1), 1–48.
- [Marder and Liu (1993)] Marder, M., Liu, Xiangming, 1993: Instability in lattice fracture. *Physical Review Letters* 71, (15), 2417–2420.
- [Mishuris, et al. (2007)] Mishuris, G.S., Movchan, A.B., Slepyan, L.I., 2007: Waves and fracture in an inhomogeneous lattice structure. *Waves in Random and Complex Media* 17, 409–428.
- [Mishuris, et al. (2008)] Mishuris, G.S., Movchan, A.B., Slepyan, L.I., 2008: Dynamical extraction of a single chain from a discrete lattice. *J. Mech. Phys. Solids* 56, 487–495.
- [Mishuris, et al. (2009a)] Mishuris, G.S., Movchan, A.B., Slepyan, L.I., 2009a: Localised knife waves in a structured interface. *J. Mech. Phys. Solids* 57, 1958–1979
- [Mishuris, et al. (2009b)] Mishuris, G.S., Movchan, A.B., Slepyan, L.I., 2009b: Localization and dynamic defects in lattice structures. *Computational and Experimental Mechanics of Advanced Materials*, CISM International Centre for Mechanical Sciences. Eds: PD Ruiz and VV Silberschmidt, Springer, 51–82.
- [Slepyan (2001a)] Slepyan, L.I., 2001a: Feeding and dissipative waves in fracture and phase transition. I. Some 1D structures and a square-cell lattice. *J. Mech. Phys. Solids* 49, 469–511.
- [Slepyan (2001b)] Slepyan, L.I., 2001b: Feeding and dissipative waves in fracture and phase transition. III. Triangular-cell lattice. *J. Mech. Phys. Solids* 49, 2839–2875.
- [Slepyan (2002)] Slepyan, L.I., 2002: *Models and Phenomena in Fracture Mechanics*. Springer, Berlin.
- [Slepyan et al. (2010)] Slepyan, L.I., Movchan, A.B., Mishuris, G.S., 2010: Crack in a lattice waveguide, *Int J Fract* 162, 91–106.

## Appendix I: The sign of $L_0$

In this section we show that for  $V \leq C_R$  and  $\alpha > 0$  the constant  $L_0$  in (4.19) of Proposition 3, section 4, is positive.

Note that by Proposition 1, for  $V_*^2 \leq C_R^2 m / \mu_2$

$$3 - 8V_*^2 > 0, \quad 2V_*^2 - 3\alpha < 0 \quad (\text{I-1})$$

and

$$V_*^4 - \frac{1}{2}(2\alpha + 1)V_*^2 + \frac{3\alpha}{8} > 0. \quad (\text{I-2})$$

Also

$$\sqrt{d_1 d_2} = 8\sqrt{3} \sqrt{V_*^4 - \frac{2\alpha + 1}{2}V_*^2 + \frac{3}{8}\left(\alpha + \frac{1}{8}\right)} > 0, \quad (\text{I-3})$$

since here the quadratic function of  $V_*^2$  was shown in the proof of Proposition 2 to be positive for  $V_*^2 \leq C_R^2 M / \mu_2$ .

**Proposition 4** For  $\alpha > 0$ ,  $V_*^2 \leq C_R^2 m / \mu_2$  the constant  $L_0$  in (4.19) is positive.

*Proof. Part 1.* Consider the cases when a)  $\alpha \geq 1$ ,  $0 < V_*^2 \leq C_R^2 m / \mu_2$  or b)  $-1/2 + \sqrt{2} \leq \alpha \leq 1$  so that  $\frac{3}{2}[\alpha - 1 + \sqrt{1 - \alpha}] \leq V_*^2 \leq C_R^2 m / \mu_2$ .

For the parameter values in both a) and b),  $M_0$  defined in (4.10) is nonnegative.

We show that  $B_1$  is negative, which implies  $B_2$  is also negative. The inequality  $B_1 < 0$  gives

$$2V_*^4 - 3(\alpha + 1)V_*^2 + \frac{9}{4}\alpha > V_*^2 M_0. \quad (\text{I-4})$$

Here, this is valid for

$$V_*^2 < \frac{3\alpha + 3 - 3\sqrt{\alpha^2 + 1}}{4},$$

which is the case, since

$$\frac{C_R^2 m}{\mu_2} = \frac{2\alpha + 1 - \sqrt{3\alpha^2 + (\alpha - 1)^2}}{4} < \frac{3\alpha + 3 - 3\sqrt{\alpha^2 + 1}}{4} \quad \text{for } \alpha > 0.$$

Indeed, the above provides us with

$$3\sqrt{\alpha^2 + 1} - \sqrt{3\alpha^2 + (\alpha - 1)^2} < \alpha + 2, \quad (\text{I-5})$$

and the left-hand side is positive as a result of

$$9(\alpha^2 + 1) > 3\alpha^2 + (\alpha - 1)^2.$$

Thus from (I-5) we have

$$(\alpha^2 + 1)(3\alpha^2 + (\alpha - 1)^2) - (2\alpha^2 - \alpha + 1) = 2\alpha^3 > 0, \quad \text{for } \alpha > 0.$$

Then (I-4) leads to

$$\frac{3}{16}(8V_*^2 - 3)(4V_*^2 - 3\alpha)^2 < 0,$$

if  $V_*^2 < 3/8$ , and this holds by Proposition 1. Therefore  $B_j < 0$ , for  $j = 1, 2$ . This together with (I-1), (I-2) and (I-3) shows  $L_0 > 0$ .  $\square$

*Part 2.* Consider the cases when a)  $0 < \alpha < -1/2 + \sqrt{2}$ ,  $0 < V_*^2 \leq C_R^2 m / \mu_2$  or b)  $-1/2 + \sqrt{2} \leq \alpha \leq 1$ ,  $0 < V_*^2 \leq \frac{3}{2}[\alpha - 1 + \sqrt{1 - \alpha}]$ .

For the parameter values in cases a) and b),  $M_0$  in (4.10) is purely imaginary and can be written as

$$M_0 = iR_0, \quad R_0 = \sqrt{3(1 - \alpha)(3\alpha - 4V_*^2) - 4V_*^4}, \quad (\text{I-6})$$

where according to the proof of Proposition 2,  $R_0^2 > 0$  since  $V_*^2 \leq C_R^2 m / \mu_2$ . Then

$$d_2 = \overline{d_1} \quad \text{and} \quad B_2 = \overline{B_1},$$

and from (4.19)

$$L_0 = \frac{|d_1| \operatorname{Re}(\overline{B_1} \sqrt{d_1})}{\sqrt{3}(3 - 8V_*^2)(2V_*^2 - 3\alpha)(V_*^4 - \frac{1}{2}(2\alpha + 1)V_*^2 + \frac{3\alpha}{8})}.$$

By (I-1), (I-2) and (I-3) it remains to show that  $\operatorname{Re}(\overline{B_1} \sqrt{d_1})$  is negative. We have

$$\operatorname{Re}(\overline{B_1} \sqrt{d_1}) = \operatorname{Re}(B_1) \operatorname{Re}(\sqrt{d_1}) + \operatorname{Im}(B_1) \operatorname{Im}(\sqrt{d_1}),$$

with

$$\operatorname{Re}(B_1) = -\frac{1}{3}V_*^4 + \frac{\alpha + 1}{2}V_*^2 - \frac{3}{8}\alpha, \quad \operatorname{Im}(B_1) = \frac{1}{6}V_*^2 R_0 > 0. \quad (\text{I-7})$$

Note that due to (I-6) and (4.9),  $-\frac{\pi}{2} < \arg(\sqrt{d_1}) < 0$ , therefore

$$\operatorname{Re}(\sqrt{d_1}) > 0, \quad \operatorname{Im}(\sqrt{d_1}) < 0. \quad (\text{I-8})$$

The roots of  $\operatorname{Re}(B_1)$  are

$$v_{\pm}^2 = \frac{3}{4}[\alpha + 1 \pm \sqrt{\alpha^2 + 1}] > 0 \quad \text{for } \alpha > 0.$$

Considering case *b*), we have

$$V_*^2 < v_-^2, \quad \text{for } 3/4 < \alpha \leq 1,$$

and then  $\operatorname{Re}(B_1) < 0$ . This with (I-7), (I-8) implies  $\operatorname{Re}(\overline{B_1} \sqrt{d_1})$  is negative and part *b*) is proved.

Returning to part *a*), for  $\operatorname{Re}(B_1) < 0$  we require

$$\frac{2\alpha + 1 - \sqrt{3\alpha^2 + (\alpha - 1)^2}}{4} < v_-^2,$$

which was shown to be valid for  $\alpha > 0$  in the proof of Proposition 2, section 4. Therefore, the proof is complete.  $\square$

## Appendix II: Poles of $L(\xi)$

Here, for  $\mu_1 = \mu_2 = 1$ , we verify the inequalities (5.10) and (5.11) of section 5, which indicate when the functions (5.8) and (5.9) are solutions of (5.1), respectively.

For  $\xi \in [0, 4\pi]$ ,  $\operatorname{sign}\{r(\Lambda_1^*)/r(\Lambda_2^*)\} = 1$  when  $\xi^2 V^2 = (\Omega_2^{(D)})^2$ . By direct substitution of (5.8) into (5.1) we obtain

$$q \Big|_{V^2 = (\Omega_2^{(D)})^2 / \xi^2} = \pm \frac{3}{2} i \sin^2(\xi/2) |\tan(\xi/2)| |4 \cos^2(\xi/2) - 1| \{T_1(\xi) - T_2(\xi)\}, \quad (\text{II-1})$$

where

$$T_j(\xi) = \operatorname{sign}\{2(1 + (-1)^j \operatorname{sign}\{\cos(\xi/2)\}) \cos^2(\xi/2) - 1\}, \quad j = 1, 2$$

and the sign in front of the right-hand side of (II-1) depends on the sign of  $r(\Lambda_1^*)$ . The factor in front of the curly braces in (II-1), is zero when  $\xi = 0, \frac{2}{3}\pi, \frac{4}{3}\pi, 2\pi, \frac{8}{3}\pi, \frac{10}{3}\pi$ , and  $4\pi$ , and is singular at  $\xi = \pi$  and  $3\pi$ .

We now show that (II-1) is zero in the neighbourhood of these poles, by solving the equation

$$T_1(\xi) - T_2(\xi) = 0.$$

For  $\xi = \pi, 3\pi$  it is clear this equation is satisfied. When  $\xi \neq \pi, 3\pi$ , we are left to determine when the inequality

$$1 - 4 \cos^2(\xi/2) > 0,$$

is satisfied. This occurs for  $\xi \in [\frac{2}{3}\pi, \frac{4}{3}\pi] \cup [\frac{8}{3}\pi, \frac{10}{3}\pi]$ . The above is confirmed in Figure 9.

Next, insertion of (5.9) into (5.1) yields

$$q \Big|_{V^2 = (\Omega_3^{(D)})^2 / \xi^2} = \frac{i\sqrt{3} \sin^2(\xi/2) |\sin(\xi/2)| (2 \cos(\xi/2) - 1 + \sqrt{3}) \sqrt{\sqrt{3} - 2 \sin^2(\xi/2)}}{2\sqrt{2 \cos^2(\xi/2) + \sqrt{3}}} \{r(\Lambda_1^*) + r(\Lambda_2^*)\}. \quad (\text{II-2})$$

The factor outside the curly braces in (II-2) has the roots  $\xi = 0, 0.7614\pi, 1.2386\pi, 2\pi, 2.7614\pi, 3.283\pi$  and  $4\pi$ . We must have  $\operatorname{sign}\{r(\Lambda_1^*)/r(\Lambda_2^*)\} = -1$  when  $V^2 \xi^2 = (\Omega_3^{(D)})^2$ . Figure 10, shows the plot of  $\operatorname{sign}\{r(\Lambda_1^*)/r(\Lambda_2^*)\}$  in this case, and we see that this condition holds provided  $\xi$  satisfies the inequalities of (5.11).



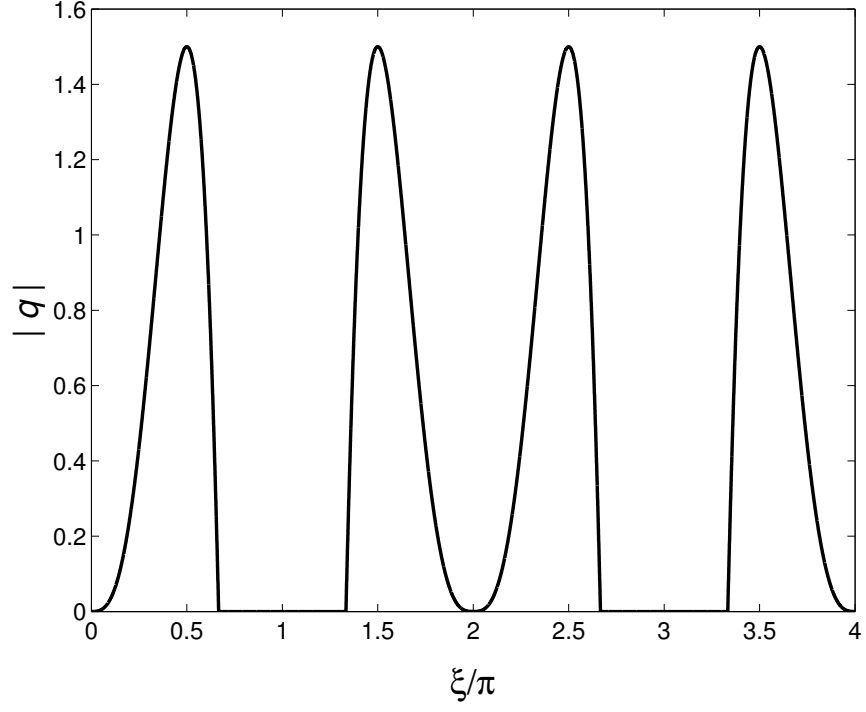


Figure 9: The plot of the absolute value of  $q$  in (II-1) as a function of the wave number, when  $V^2\xi^2 = (\Omega_2^{(D)})^2$ .

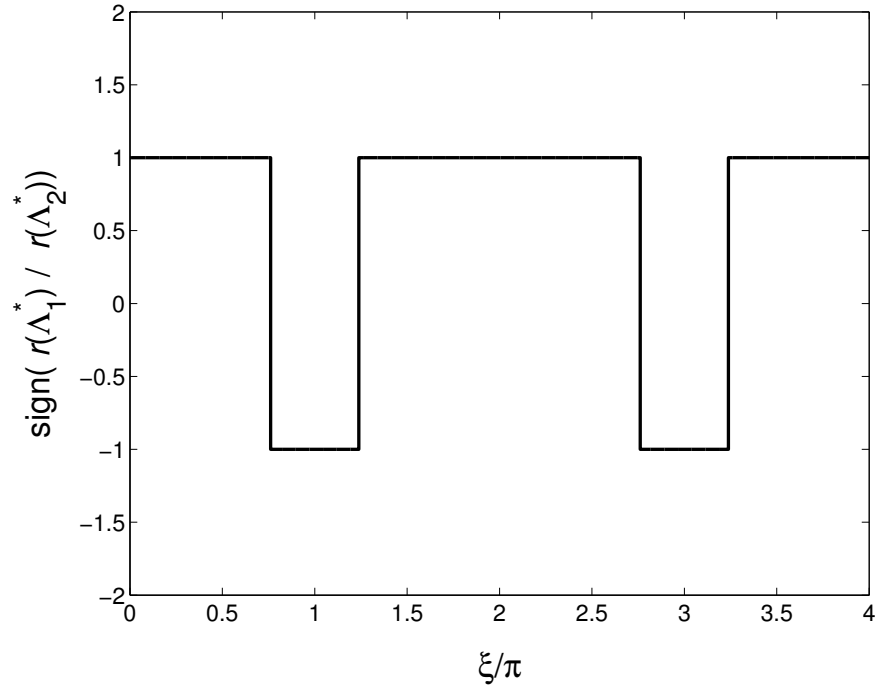


Figure 10: The sign of the ratio of  $r(\Lambda_1^*)$  to  $r(\Lambda_2^*)$  as a function of  $\xi/\pi$ , when  $V^2\xi^2 = (\Omega_3^{(D)})^2$ .

### Appendix III: Asymptotic properties of $L(\xi)$

We now state and prove some properties of the kernel function  $L(\xi)$ , which are used in the analysis of the Wiener-Hopf equation (4.5), in section 6.

**Lemma 1**  $L(\xi) \rightarrow 1$  as  $|\xi| \rightarrow \infty$ .

*Proof.* According to (4.11), for  $|\xi| \rightarrow \infty$ , we have

$$\begin{aligned} \Lambda_j^* &= \frac{1}{2z_j} + O(|z_j|^{-3}), \quad \text{and} \quad r(\Lambda_j^*) = 1, j = 1, 2, \\ \sqrt{z_j^2 - 1} &= z_j + O(|z_j|^{-1}), \\ F(z_j) &= 3z_j^2 - \frac{m}{\mu_2}(\varepsilon + i\xi V)^2 z_j [2 \cos(\xi/2) + 1] + O(|\xi|^2). \end{aligned} \tag{III-1}$$

Since  $z_j = O(|\xi|^2)$  for  $|\xi| \rightarrow \infty$ , then

$$\begin{aligned} F(z_2)\sqrt{z_1^2 - 1} - F(z_1)\sqrt{z_2^2 - 1} &= 3z_1z_2(z_2 - z_1) + O(|\xi|^4), \\ 3(z_2 - z_1)\sqrt{z_1^2 - 1}\sqrt{z_2^2 - 1} &= 3z_1z_2(z_2 - z_1) + O(|\xi|^2). \end{aligned}$$

The leading order term in both of the above estimates is  $O(|\xi|^6)$  for  $|\xi| \rightarrow \infty$ , therefore

$$L(\xi) = 1 + O(|\xi|^{-2}), \quad |\xi| \rightarrow \infty.$$

□

Next we state

**Lemma 2** For the product of two complex functions  $f(\xi), g(\xi) \in \mathcal{J}$ , we have  $(fg)(\xi) \in \mathcal{J}$ .

This leads to

**Lemma 3** For  $\xi \in \mathbb{R}$ , for  $\varepsilon > 0$ ,  $L(\xi) \in \mathcal{J}$ .

*Proof.* The term

$$\frac{m}{\mu_2}(\varepsilon^2 - \xi^2 V^2 + 2i\xi\varepsilon V) \in \mathcal{J}$$

since it has an even real part and odd imaginary part with respect to  $\xi$ . This together with Lemma 2 and (3.5) shows that  $z_j \in \mathcal{J}$ ,  $j = 1, 2$ . and hence, after a second application of Lemma 2 with (4.6) we complete the proof.

Now we consider the index of the function  $L(\xi)$  which defined by

$$\text{Ind}(L(\xi)) = \frac{1}{2\pi} [\arg(L(\infty)) - \arg(L(-\infty))]. \tag{III-2}$$

This quantity can also be interpreted as the number of times the path traced by  $L(\xi)$  in the complex plane for  $\xi \in (-\infty, \infty)$  winds around the origin. We have

**Lemma 4** For  $\varepsilon > 0$ , we have  $\text{Ind}(L(\xi)) = 0$ .

*Proof.* According to section 6, if  $\xi = \xi^*$  represents a root or a pole of  $L(\xi)$  such that  $V < V_g$  ( $V > V_g$ ), then the regularisation parameter  $\varepsilon$  shifts this root or pole into lower (upper) half of the complex plane. Correspondingly,  $\xi = -\xi^*$  is then a root or a pole of  $L(\xi)$  such that  $V > V_g$  ( $V < V_g$ ) and this will be located in the upper (lower) half of the complex plane after the regularisation of  $L(\xi)$ . Therefore,  $L(\varepsilon + i\xi V, \xi)$  has an equal number of roots in the upper and lower half planes and an equal number of poles in the upper and lower half planes, and these numbers are independent of  $\varepsilon$ . Hence it is sufficient to show that for large  $\varepsilon$ ,  $\text{Ind}(L(\varepsilon + i\xi V, \xi)) = 0$ .

First assume  $\xi, \varepsilon \gg 1$ , so that  $|\varepsilon + i\xi V| \gg 1$ , then

$$z_j = O(\varepsilon^2 + \xi^2 V^2), \quad \Lambda_j^* = \frac{1}{2z_j} + O\left(\frac{1}{(\varepsilon^2 + \xi^2 V^2)^3}\right),$$

and so

$$r(\Lambda_j^*) = 1, \quad 3(z_2 - z_1)\sqrt{z_1^2 - 1}\sqrt{z_2^2 - 1} = 3z_1 z_2(z_2 - z_1) + O(\varepsilon^2 + \xi^2 V^2),$$

and

$$\begin{aligned} & F(z_2)\sqrt{z_1^2 - 1} - F(z_1)\sqrt{z_2^2 - 1} \\ &= 3z_1 z_2(z_2 - z_1) - \frac{m}{\mu_2}(\varepsilon + i\xi V)^2(z_2 - z_1)(2 + \cos(\xi/2)) + O(\varepsilon^2 + \xi^2 V^2). \end{aligned}$$

Thus, from (4.6),

$$L(\varepsilon + i\xi V, \xi) = 1 + \frac{m(\varepsilon + i\xi V)^2[2 + \cos(\xi/2)]}{3\mu_2 z_1 z_2} + O\left(\frac{1}{(\varepsilon^2 + \xi^2 V^2)^2}\right), \quad \varepsilon^2 + \xi^2 V^2 \rightarrow \infty, \quad (\text{III-3})$$

where according to (3.5),  $z_1 z_2$  is  $O((\varepsilon^2 + \xi^2 V^2)^2)$ . The remainder estimate here is uniform for large  $\varepsilon$  and  $\xi$ .

The plot of the contour traced by  $L(\xi)$  for large  $\varepsilon$  and  $\xi$ , with  $m = \mu_1 = \mu_2 = 1$  ( $\alpha = 1$ ),  $V = 0.3941$ , can be found in Figure 11. In this figure both the plot given by (4.6) and the leading order term of (III-3) are presented, and it can be seen there is a good agreement between both computations. When  $\varepsilon \gg \xi$ , from (III-3)

$$L(s + i\xi V, \xi) = 1 + \frac{\mu_2(2 + \cos(\xi/2))}{m} \left[ \frac{1}{\varepsilon^2} - \frac{2i\xi V}{\varepsilon^3} \right] + O\left(\frac{1}{\varepsilon^4}\right), \quad \varepsilon \rightarrow \infty,$$

and this asymptotic expression (III-3) implies that for large  $\varepsilon$  the contour traced by  $L$  does not cross the negative real axis, since to leading order the above real part is always positive, whereas the imaginary part can cross the real axis for  $\xi \in (-\infty, \infty)$ . Similar behaviour can be seen in Figure 11, where the contour traced by  $L(\varepsilon + i\xi V, \xi)$  for  $\xi \in (-400\pi, 400\pi)$  in the complex plane forms a closed loop which passes through 1. Therefore,  $\text{Ind}(L(\varepsilon + i\xi V, \xi)) = 0$  in the limit  $\varepsilon \rightarrow \infty$  and this also holds for all  $\varepsilon > 0$ .  $\square$

The next two corollaries provide us with additional properties of  $L(\xi)$  needed for the factorisation of (4.5). As a corollary of Lemma 3 we have

**Corollary 1** For  $\xi \in \mathbb{R}$ ,  $\varepsilon > 0$ ,

$$\arg(L(\xi)) = -\arg(L(-\xi)).$$

Owing to (III-2), Lemma 4 and Corollary 1 we also have:

**Corollary 2**  $\arg(L(\xi)) = 0$  as  $\xi \rightarrow \pm\infty$ .

## Appendix IV: Solution of the Wiener-Hopf equation (6.3) for a particular load

In order to determine the functions  $\mathcal{S}_+$  and  $\mathcal{S}_-$ , as solutions of the Wiener-Hopf equation (6.3), for the sake of simplicity, we consider a certain type of “load”  $\phi^F$  which produces simple examples for the additive split  $P_+ + P_-$  in the right-hand side of (6.3).

Let  $\mathcal{P}_+$  ( $\mathcal{P}_-$ ) be the set of poles and  $\mathcal{Z}_+$  ( $\mathcal{Z}_-$ ) the set of zeros of  $L(\varepsilon + i\xi V, \xi)$  that are located in the upper (lower) half plane. The first factor in the right-hand side of (6.3) is singular at the zeros of  $L_-$  and the singular points of  $L_+$ . Assume  $\xi_p^- \in \mathcal{P}_-$ , and

$$L_+(\varepsilon + i\xi V, \xi) \sim \frac{A_p}{[\zeta_- \varepsilon - i(\xi - \xi_p^-)]^a}, \quad a > 0, \varepsilon \rightarrow +0, \quad (\text{IV-1})$$

where  $\zeta_- = 1/(V_g - V)$  for  $\xi \rightarrow \xi_p^-$ . Also, suppose for  $\xi_z^+ \in \mathcal{Z}_+$

$$L_-(\varepsilon + i\xi V, \xi) \sim A_z[\zeta_+ \varepsilon - i(\xi - \xi_z^+)]^b, \quad b > 0, \varepsilon \rightarrow +0, \quad (\text{IV-2})$$

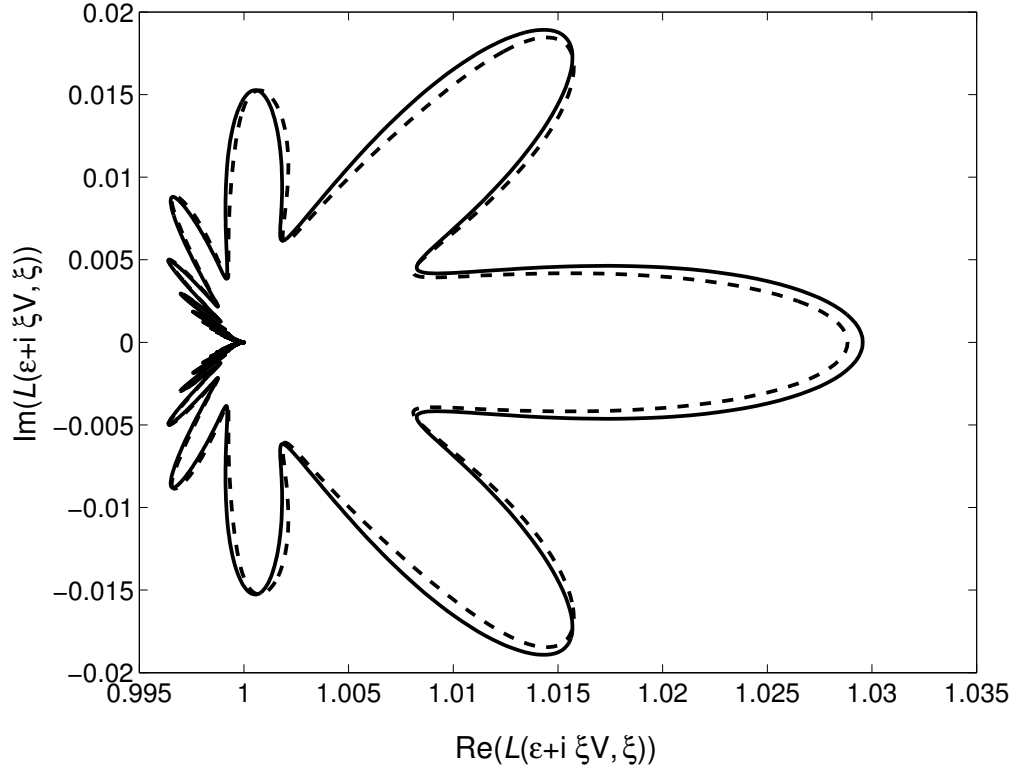


Figure 11: The contour traced by  $L(\varepsilon + i\xi V, \xi)$  in the complex plane for  $\varepsilon = 10$ ,  $m = \mu_1 = \mu_2 = 1$ ,  $(\alpha = 1)$ ,  $V = 0.3941$ ,  $\xi/\pi \in (-400, 400)$ . The computations for the solid curve are based on formula (4.6) and those for the dashed curve are based on the leading order part of (III-3).

for  $\xi \rightarrow \xi_z^+$  and  $\zeta_+ = 1/(V - V_g)$ . Here,  $\xi_p^-$  is a pole and  $\xi_z^+$  is a zero of  $L$  located in the lower and upper half of the complex plane, respectively, and the constants  $A_p$  and  $A_z$  depend on  $\alpha$ .

We consider two examples of the function  $\phi$ :

a)

$$\phi_A(\eta) = \phi(\eta) = -\mathcal{C}_A(2\zeta_-\varepsilon)^a \exp[(\zeta_-\varepsilon - i\xi_p^-)\eta] H(-\eta) , \quad (\text{IV-3})$$

and after taking the Fourier transform, we have

$$\phi_{A,-} = -\frac{(2\zeta_-\varepsilon)^a \mathcal{C}_A}{[\zeta_-\varepsilon + i(\xi - \xi_p^-)]} , \quad \phi_{A,+} = 0 , \quad (\text{IV-4})$$

and b)

$$\phi_B(\eta) = q(\eta) = \mathcal{C}_B(2\zeta_+\varepsilon)^b \exp[-(\zeta_+\varepsilon + i\xi_z^+)\eta] H(\eta) .$$

so that

$$\phi_{B,+} = \frac{(2\zeta_+\varepsilon)^b \mathcal{C}_B}{[\zeta_+\varepsilon - i(\xi - \xi_z^+)]} , \quad \phi_{B,-} = 0 . \quad (\text{IV-5})$$

In cases a) and b), we have  $\mathcal{C}_A$  and  $\mathcal{C}_B$  are constants representing the intensity of the load. Also

$$\lim_{\varepsilon \rightarrow +0} \phi_A(\eta) = \lim_{\varepsilon \rightarrow +0} \phi_B(\eta) = 0 . \quad (\text{IV-6})$$

*Right-hand side of (6.3) for the load of case a).* We insert (IV-4) into (6.3) and taking the limit as  $\varepsilon \rightarrow +0$  and noting that due to (IV-6)

$$\lim_{\varepsilon \rightarrow +0} \frac{\phi_{A,-}}{L_-} = 0 ,$$

we have using (IV-1):

$$L_+ \mathcal{S}_+ + \frac{\mathcal{S}_-}{L_-} = A_p \mathcal{C}_A \lim_{\varepsilon \rightarrow +0} \frac{(2\zeta_-\varepsilon)^a}{[\zeta_-\varepsilon - i(\xi - \xi_p^-)]^a [\zeta_-\varepsilon + i(\xi - \xi_p^-)]} .$$

Here, according to [Slepyan (2002), Section 2.2.4], the above limit converges to the Dirac delta function, therefore

$$L_+ \mathcal{S}_+ + \frac{\mathcal{S}_-}{L_-} \sim 2\pi A_p \mathcal{C}_A \delta(\xi - \xi_p^-) = A_p \mathcal{C}_A \left[ \frac{1}{\varepsilon + i(\xi - \xi_p^-)} + \frac{1}{\varepsilon - i(\xi - \xi_p^-)} \right] , \quad \varepsilon \rightarrow +0 .$$

*Right-hand side of (6.3) for the load of case b).* Similarly, using (IV-2), (IV-5) and

$$\lim_{\varepsilon \rightarrow +0} \phi_{B,+} L_+ = 0 ,$$

by [Slepyan (2002), Section 2.2.4], we have

$$\begin{aligned} L_+ \mathcal{S}_+ + \frac{\mathcal{S}_-}{L_-} &= \lim_{\varepsilon \rightarrow +0} \frac{\mathcal{C}_B}{A_z} \frac{(2\zeta_+\varepsilon)^b}{[\zeta_+\varepsilon + i(\xi - \xi_z^+)]^b [\zeta_+\varepsilon - i(\xi - \xi_z^+)]} \\ &\sim 2\pi \frac{\mathcal{C}_B}{A_z} \delta(\xi - \xi_z^+) = \frac{\mathcal{C}_B}{A_z} \left[ \frac{1}{\varepsilon + i(\xi - \xi_z^+)} + \frac{1}{\varepsilon - i(\xi - \xi_z^+)} \right] , \quad \varepsilon \rightarrow 0 . \end{aligned}$$

*General solution of (6.3).* Consulting the above cases a) and b), by linear superposition the right-hand side of (6.3) has the form

$$L_+ \mathcal{S}_+ + \frac{\mathcal{S}_-}{L_-} = \sum_{\xi_p \in \mathcal{P}_-} \mathcal{A}_p \left[ \frac{1}{\varepsilon + i(\xi - \xi_p)} + \frac{1}{\varepsilon - i(\xi - \xi_p)} \right] + \sum_{\xi_z \in \mathcal{Z}_+} \mathcal{B}_z \left[ \frac{1}{\varepsilon + i(\xi - \xi_z)} + \frac{1}{\varepsilon - i(\xi - \xi_z)} \right] ,$$

for  $\varepsilon \rightarrow 0$ , where  $\mathcal{A}_p$  and  $\mathcal{B}_p$  are arbitrary complex constants.

Then the functions  $\mathcal{S}_+$  and  $\mathcal{S}_-$  are given by

$$\begin{aligned}\mathcal{S}_+ &= \frac{1}{L_+(\xi)} \left[ \sum_{\xi_p \in \mathcal{P}_-} \frac{\mathcal{A}_p}{\varepsilon - i(\xi - \xi_p)} + \sum_{\xi_z \in \mathcal{Z}_+} \frac{\mathcal{B}_z}{\varepsilon - i(\xi - \xi_z)} \right], \\ \mathcal{S}_- &= L_-(\xi) \left[ \sum_{\xi_p \in \mathcal{P}_-} \frac{\mathcal{A}_p}{\varepsilon + i(\xi - \xi_p)} + \sum_{\xi_z \in \mathcal{Z}_+} \frac{\mathcal{B}_z}{\varepsilon + i(\xi - \xi_z)} \right],\end{aligned}\tag{IV-7}$$

where  $\varepsilon \rightarrow +0$ . In section 6, (6.4) follows by considering terms in (IV-7) which correspond  $p_- = 0$  and  $\nu = 1/2$  in (IV-2) and (IV-3).

## Appendix V: Evaluation of $L_{\pm}$ for $\xi \rightarrow 0$

Now, using the Cauchy-type integral of (6.2) and the asymptotic representation (4.18) for  $L$  when  $\xi \rightarrow 0$ , we derive asymptotes of the functions  $L_{\pm}$  near zero, found in (7.2). The logarithmic term in (6.2) is rewritten as

$$\ln L(\varepsilon + i\xi V, \xi) = \ln |L(\varepsilon + i\xi V, \xi)| + i \arg(L(\varepsilon + i\xi V, \xi)).$$

Then

$$\begin{aligned}L_{\pm}(\varepsilon + i\xi V, \xi) &= \exp\left(\pm \frac{1}{2\pi i} \int_{-\infty}^{\infty} \frac{\ln |L(\varepsilon + isV, s)|}{s - \xi} ds\right) \\ &\quad \times \exp\left(\pm \frac{1}{2\pi} \int_{-\infty}^{\infty} \frac{\arg(L(\varepsilon + isV, s))}{s - \xi} ds\right).\end{aligned}\tag{V-1}$$

The first exponent on the right, by the Cauchy theorem, defines the modulus of  $L(\varepsilon + i\xi V, \xi)$ , whereas the second exponent, owing to the expansion

$$\frac{1}{s - \xi} = \sum_{n=0}^{\infty} \frac{\xi^n}{s^{n+1}}$$

yields

$$\exp\left(\pm \frac{1}{2\pi} \int_{-\infty}^{\infty} \frac{\arg(L(\varepsilon + isV, s))}{s - \xi} ds\right) \sim \exp\left(\pm \frac{1}{2\pi} \int_{-\infty}^{\infty} \frac{\arg(L(\varepsilon + isV, s))}{s} ds\right).$$

The integrand in the right-hand side is an even function as a result of Corollary 1, and so

$$\exp\left(\pm \frac{1}{2\pi} \int_{-\infty}^{\infty} \frac{\arg(L(\varepsilon + isV, s))}{s - \xi} ds\right) \sim \exp\left(\pm \frac{1}{\pi} \int_0^{\infty} \frac{\arg(L(\varepsilon + isV, s))}{s} ds\right).$$

Therefore, allowing  $\varepsilon \rightarrow +0$  in (V-1), and using Proposition 3, we obtain (7.2).